UNIVERSITY OF CALIFORNIA,
IRVINE

The Role of Neuromodulatory Projections from the Basal Forebrain Area to the Primary Visual Cortex of the Rodent

DISSERTATION

submitted in partial satisfaction of the requirements
for the degree of

DOCTOR OF PHILOSOPHY

in Psychology

by

Georgina Alexandra Lean

Dissertation Committee:
Professor David C. Lyon, Chair
Professor Emily Grossman
Professor Jeffrey Krichmar

2019

DEDICATION

To

my family, who have supported me

throughout my unusual journey to

discover my passion.

TABLE OF CONTENTS

	Page
LIST OF FIGURES	iv
LIST OF TABLES	vi
ACKNOWLEDGMENTS	vii
CURRICULUM VITAE	viii
ABSTRACT OF THE DISSERTATION	ix
INTRODUCTION	1
CHAPTER 1: Cell Type Specific Tracing of the Subcortical Input to Primary Visual Cortex from the Basal Forebrain	16
CHAPTER 2: Enhanced Method for Cell-Type Specific Tracing Confirms Inhibitory Neurons are the Primary Target of the Basal Forebrain Inputs to Primary Visual Cortex	33
CHAPTER 3: Size Tuning Effects with Optogenetic Manipulation of Basal Forebrain Projection Neurons to V1 Recipients in Rodent	49
CHAPTER 4: Summary and Conclusions	63
REFERENCES	67

LIST OF FIGURES

Page

Figure 0.1 Major Cholinergic Projections to Central Nervous System 2

Figure 0.2 Distribution of mAChR's Across V1 Cortical Layers 6

Figure 0.3 Single-Cell Recordings with External Acetylcholine Application 9

Figure 1.1 Schematic of Basal Forebrain Projection to Mouse V1 18

Figure 1.2 Cell Type Specific Tracing Schematic 19

Figure 1.3 Digital Images of Virus Injection Site in V1 22

Figure 1.4 Example of Basal Forebrain Labeling Following ΔG-RV in Mouse V1 24

Figure 1.5 Example of Basal Forebrain Labeling Following AAV-GAD-YTB and Subsequent EnvA-ΔG-RV in Mouse V1 24

Figure 1.6 Example of Basal Forebrain Labeling Following LV-αCamKII-YTB and Subsequent EnvA-ΔG-RV in Mouse V1 25

Figure 1.7 Summary of Cell Type Specific Basal Forebrain Input to V1 29

Figure 2.1 Reconstruction of AAV-GAD-YToG and LV-aCamKII-YToG injection site 40

Figure 2.2 Reconstruction of Retrograde Infected Neurons using YToG 41

Figure 2.3 Additional Reconstruction of LV-aCamKII-YToG Injection 43

Figure 2.4 Schematic Representation of Relative Strength of YTB and YToG 46

Figure 3.1 Diagram of G-Deleted Rabies Virus 52

Figure 3.2 Summary Figure of Electrophysiological and Optogenetic Recording Methods 55

Figure 3.3 Choline Acetyltransferase Labeling in Basal Forebrain 57

Figure 3.4 Comparison of Firing Rate and Size Patterns 58

Figure 3.5 Graphical Representation of Aperture Tuning versus Firing Rate with 3 Different Laser Conditions 59

Figure 3.6 Average Firing Rate at Different Cortical Depths 60

LIST OF TABLES

Page

Table 1.1 Number of Retrogradely Infected Neurons in LGN and Basal Forebrain Following ΔG-RV injection in V1 26

Table 1.2 Number of Retrogradely Infected Neurons in LGN and Basal Forebrain Following Cell-type Specific Promoter injections in V1 28

Table 2.1 Comparison of Retrograde Infected Neurons Using YTB and YToG 42

Table 2.2 Average Cell Counts for Each Region 45

ACKNOWLEDGMENTS

I would like to express my deepest appreciation to my committee chair, Dr. David Lyon, for his patience and understanding as I found my way, both in and out of the lab.

I would like to thank my committee members, Dr. Emily Grossman and Dr. Jeff Krichmar, for their continued support and constant guidance throughout my time at UC, Irvine.

Additionally, I owe a deep gratitude to Drs. Yongjun Liu and Andrzej Foik for their assistance throughout this project, both with acquisition and analysis of data as well as instruction and method development. I truly could not have accomplished this task without their aid, and I thank them.

The text in chapter 1 of this dissertation is a reprint of the material as it appears in the Journal of Comparative Neurology. The co-authors listed in this publication directed and supervised research which forms the basis for this dissertation.

CURRICULUM VITAE

Georgina Alexandra Lean

2010-13 Research Assistant, Larry Swanson Lab, Dornsife College of Letters, Arts, and Sciences, University of Southern California, Los Angeles, California

2013 B.S. in Neurosciences, University of Southern California

2014-18 Teaching Assistant, Graduate School of Social Science, University of California, Irvine

2014-18 Research Assistant, Graduate School of Social Science, University of California, Irvine

2016 M.S. in Cognitive Neuroscience, University of California, Irvine

2019 Ph.D. in Psychology with a Concentration in Neuroscience
University of California, Irvine
Dissertation: "The Role of Neuromodulatory Projections from the Basal Forebrain Area to the Primary Visual Cortex of the Rodent"
Professor David C. Lyon, Chair

FIELD OF STUDY

Projections to visual cortical neurons from subcortical regions in rodent models.

PUBLICATIONS

Lean, G.A., Liu, Y.J., & Lyon, D.C. (2019) Cell type specific tracing of the subcortical input to primary visual cortex from the basal forebrain. *J Comp Neurol.,* 527(3). https://doi.org/10.1002/cne.24412

Lean, G.A., Liu, Y.J., & Lyon, D.C. (2016, November). *Basal forebrain provides direct projections to inhibitory neurons in mouse primary visual cortex, but not to the parvalbumin-positive inhibitory subtype.* Poster presented at the Society for Neuroscience Conference, San Diego, CA.

Lean, G.A., Liu, Y.J., & Lyon, D.C. (2015, November). *Cell-type specific tracing of the subcortical input to primary visual cortex from the hypothalamus.* Poster presented at the Society for Neuroscience Conference, Chicago, IL.

ABSTRACT OF THE DISSERTATION

The Role of Neuromodulatory Projections from the
Basal Forebrain Area to the Primary Visual Cortex of the Rodent

Georgina Alexandra Lean

Doctor of Philosophy in Psychology

University of California, Irvine, 2019

Professor David C. Lyon, Chair

Neuroanatomical studies play a key role in developing an understanding of neural connectivity and providing insight into how structure leads to function. Cell-type specific tracing methods have been utilized to identify distinct projection neurons originating from the basal forebrain and terminating in the primary visual cortex (V1). These neurons have been exclusively labeled using cell type-specific helper viruses, which allow for selective infection and spread of modified rabies viruses to label the projection neurons terminating onto specific neuron types in V1. While basal forebrain afferents terminate in the infragranular layers of V1, acetylcholine is delivered to more superficial layers through volume transmission. This study was designed to determine the synaptic targets and functional implications of this projection pathway utilizing a retrograde-tracing method to deliver light-gated ion channels to basal forebrain projection neurons. This allowed for direct optogenetic manipulation during single unit recording in V1 of anaesthetized rats. In doing so, we found significant suppression of cell response to the preferred stimulus with basal forebrain activation. Conversely, we found that responses to stimuli smaller than the optimal size were facilitated during basal forebrain activation. Thus, basal forebrain effects on V1 neurons depend on stimulus size. We examine the differences among cortical layers to

further distinguish the role acetylcholine plays in the cortex. provide insight into the mechanism of cholinergic modulation from visual processing.

INTRODUCTION

A variety of neural structures contribute to the brain's ability to process and understand the multitude of stimuli in the environment. Our cognitive abilities stem from the inherent and complex interactions between these structures. Upon examination, we can find specific patterns of interactions and identify key pathways to further our understanding of how the brain can process any and all stimuli.

Visual processing utilizes these complex pathways and involves the interaction of a wide range of brain regions. The retina receives visual stimuli and translates each component into electrical signals that trigger specific cells in the primary visual cortex to fire based on the size and orientation of the stimulus. The primary visual cortex (V1) is comprised of a series of cells arranged in such a way as to fire with an optimal stimulus presentation, known as the cell's classical receptive field (Sceniak et al., 1999; Angelucci et al., 2002; Cavanaugh et al., 2002). Each cell is mediated by center/surround suppression modulation which has significant effects on fundamental visual processes in V1, such as orientation tuning, contrast sensitivity and size tuning (Sceniak et al., 1999; Chen et al., 2005; Hashemi-Nezhad and Lyon, 2012; Liu et al., 2015) and is thought to play a critical role in early object perception processed in higher visual areas (Series et al., 2003). The method of center/surround suppression is understood on a functional level; however, the detailed physiological mechanisms that influence this process are still being determined.

One of the more recently discovered contributions to this pathway is the projection from the basal forebrain area to the primary visual cortex. The basal forebrain is predominantly characterized by its' cholinergic projection patterns to the cortex (Newman et al., 2012). Given

the high density of cholinergic varicosities within V1 (Lysakowski et al., 1989; Mechawar et al., 2000) and the functional contribution of acetylcholine to plasticity in V1 (Bear and Singer, 1986), acetylcholine from the basal forebrain is particularly well-suited to reinforce V1 (Chubykin et al., 2013).

Characteristics of the Basal Forebrain:

The basal forebrain is a broad term used to describe a large subcortical region at the base of the brain defined by the presence of clusters of cholinergic (Ch) neurons (Meynert, 1872). It is classically divided into four subregions based on these cholinergic clusters: the medial septum (Ch1), the vertical limb of the diagonal band (Ch2), the horizontal limb of the diagonal band (Ch3), and the substantia innominata/nucleus basalis (Ch4) (See figure 0.1 for a schematic representation of these subregions and their main projection targets; Lin et al., 2015). One of the difficulties in reviewing the literature about this region is the lack of systematic nomenclature

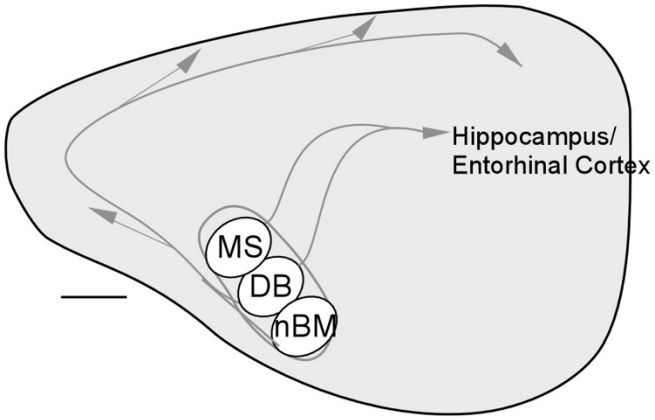

Figure 0.1: Schematic representation of cholinergic projections from the basal forebrain to the central nervous system. There are two groups of projections: one originating from the magnocellular basal forebrain cholinergic system (depicted here) and the brainstem cholinergic system (not included in this figure). The basal forebrain cholinergic system is comprised of four distinct subregions based on their cholinergic clusters: the medial septal nucleus (MS), the vertical and horizontal limbs of the diagonal band of Broca (DB), and the nucleus basalis magnocellularis (nBM). The MS and vertical limb of the DB project to the hippocampus and entorhinal cortices. The horizontal limb of the DB and the nBM project to the neocortex, as well as the basolateral amygdala and olfactory bulbs (not shown). Pathways shown here are based on Newman et al., 2012.

among studies; as such, the literature often refers to the same region using several different names and compounds the ability to truly rely on the qualitative results. Additionally, the development of a specific chemical target for cholinergic neurons was not available for early studies of this area (Everitt and Robbins, 1997). However, recent advances in chemoarchitectural mechanisms and the use of genetically modified animals have enhanced the verifiability of neuroanatomical studies involving this region.

Each subregion is characterized primarily via its' cell morphology and the cortical afferents. The Ch1 cell group is characterized by relatively small cell types (Mesulam et al., 1983b) and projections into the hippocampus (Newman et al., 2012). The Ch2 group, originating in the vertical limb of the diagonal band of Broca, is also found to target the hippocampus (Newman et al., 2012) and is classified by larger cell bodies and more oblong shapes (Mesulam et al., 1983b). The Ch3 cell group is located in the horizontal limb of the diagonal band of Broca and has mostly a medium-sized cell type (Mesulam et al., 1983b). The Ch4 cell group, also known as the nucleus basalis of Meynert, is the most extensive of the basal forebrain cholinergic subgroups. The main projection target from this region is to the neocortex and basolateral amygdala (Newman et al., 2012). Combined, these four distinct subregions project to the hippocampus, olfactory bulb, neocortex, and basolateral amygdala (Newman et al., 2012).

Evidence for the Basal Forebrain projection to V1:

Though cortical projections from the basal forebrain were identified some time ago (Meynert, 1872), a specific projection to visual areas was not confirmed until relatively recently. The cholinergic nature of the basal forebrain led Shute and Lewis to suggest its' role in cholinergic innervation of the cortex (Shute and Lewis, 1967). This connection was then

confirmed in 1981 when Henderson provided evidence for a projection from "acetylcholinesterase-containing neurones in the diagonal band to the occipital cortex of the rat" using the retrograde tracer, horseradish peroxidase (HRP) (Henderson, 1981). Shortly after, Tigges et al. (1982) provided evidence for a similar subcortical projection to visual cortex in squirrel monkey, suggesting that this projection is "phylogenetically stable." Since then, a number of studies have confirmed this projection to visual cortex from the ipsilateral and contralateral claustrum, the horizontal limb of the diagonal band of Broca, the lateral preoptic area of the hypothalamus, and the septum (Carey and Rieck, 1987; Dreher et al., 1990; Do et al., 2016).

A functional study further confirmed the projection to be necessary for many visual cortical cells to respond to visual stimuli presentation. Following lesions in the basal forebrain, Sato et al. (1987a) found that many V1 neurons no longer responded to the stimulus presented. Importantly, iontophoretic application of acetylcholine facilitated visual responses in the majority of cells that were diminished following lesions to the basal forebrain, indicating that the projection to visual cortex is critical for visual processing due to its' role in providing acetylcholine to V1.

Cholinergic Receptors in the Visual Cortex:

Acetylcholine has been implicated in a variety of neurological functions, including sensory processing, learning, arousal, attention, and awareness (Everitt and Robbins, 1997; Sarter et al., 2001; Roberts et al., 2005). The mechanism of synaptic transmission with cholinergic fibers is unique in that there is not always a direct synapse between a cholinergic fiber and postsynaptic dendrites (Umbriaco et al., 1994). Rather, acetylcholine can influence

neurons via diffuse extrasynaptic modulation known as volume transmission (Descarries et al., 1997; Sarter et al., 2009). As such, determining which neurons in the circuit are receptive to ACh is a critical step in understanding the role of cholinergic modulation in visual processing (Disney et al., 2012).

The two main classes of acetylcholine receptors (AChRs) are distinguished by their activating substrate (muscarine or nicotine) and are named accordingly. Nicotinic AChRs (nAChRs) are primarily found presynaptically at thalamic synapses onto excitatory neurons in layer 4c and thus play a dominant role in cholinergic modulation of thalamocortical transmission and affect neuronal gain (Disney et al., 2007). Elsewhere in V1, nAChRs are expressed mainly on GABAergic interneurons. Disney et al. (2007) found that 75% of the cells labeled with nAChRs were GABAergic; yet this only comprised a small proportion (~7%) of V1 neurons overall. As such, the predominant role of nAChRs is considered to be excitatory modulation of layer 4c neurons from the thalamus.

The projection from the basal forebrain is considered to be primarily targeted to the second class of acetylcholine receptors. Muscarinic AChRs (mAChRs) are further divided into 5 subtypes, differentiable via immunohistochemistry (Newman et al, 2012). The m1 receptor is predominantly located at postsynaptic sites and mediates depolarization and suppression of spike-frequency accommodation (Dasari and Gulledge, 2011). Both the m1 and m2 receptors are known to be strongly expressed in the neocortex of monkeys (Mrzljak et al., 1993; Tigges et al., 1997) and were used as the targets in a characterization study of AChRs in visual cortex.

Since both acetylcholine receptor types are found on glutamatergic and GABAergic interneurons in the cortex (Disney et al., 2006), measuring electrical activity alone is insufficient to determine the particular role of cholinergic projections on a target area. Instead, a quantitative

measure of AChRs across glutamatergic and GABAergic cells provides more insight into the modulatory role. Using dual immunofluorescence labeling to distinguish GABAergic neurons and particular AChR subtypes, Disney et al (2006) were able to determine receptor frequency. Since 20% of the cells across all layers in V1 are GABAergic, one would expect a similar distribution of AChRs if the cholinergic projection was equally targeted toward excitatory and inhibitory cells. Instead, Disney et al. found a higher rate of m1 and m2 acetylcholine receptor expression from GABAergic neurons in macaque V1 across all cortical layers; 60% of cells with m1 receptors and 52% with m2 receptors were GABAergic (Figure 0.2; Disney et al., 2006). Therefore, cholinergic release in V1 primarily activates inhibitory neurons, with the exception of excitatory modulation in layer 4c from nAChRs.

This immunohistochemical analysis confirms prior results, which showed direct modulation by acetylcholine in V1. Application of the muscarinic antagonist atropine suppressed visual responses in V1 cells that were facilitated by acetylcholine, suggesting that endogenous

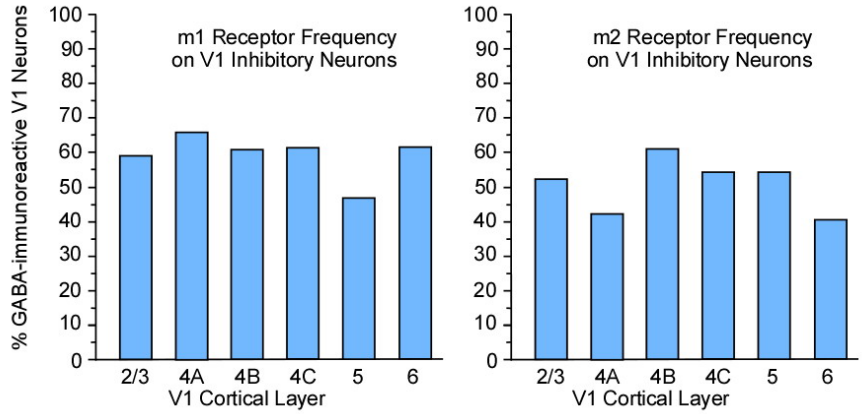

Figure 0.2 : Proportion of cells in V1 with muscarinic acetylcholine receptors (mAChRs) that are GABA immunoreactive. The graph on the left shows immunoreactivity of m1 AChRs compared with GABA immunoreactivity (n=1833), while the graph on the right shows immunoreactivity of m2 AChRs compared with GABA immunoreactivity (n=1790). Given the known proportion of GABAergic neurons in V1 is approximately 20% of all V1 cells, one would assume that the proportion of cells with AChRs that are GABAergic would be approximately 20% if there is an equal distribtution of AChRs among excitatory and inhibitory cell types. Instead, this data indicates increased expression of AChRs among inhibitory neurons. Based on data from Disney et al., 2006.

acetylcholine release may modulate visual responsivity in cortical neurons (Sato et al., 1987b). The importance of this relationship between acetylcholine and visual response facilitation lies in V1's role in processing visual information.

The Role of Inhibitory Interneurons in visual processing:

Cells in V1 are known to respond preferentially to a stimulus appearing within the cell's classical receptive field (Sceniak et al., 1999; Cavanaugh et al., 2002; Roberts et al., 2005). The majority of naturally viewed stimuli, however, do not fall perfectly into a cell's receptive field. In order to accommodate the wide range of visual stimuli we are exposed to, the visual cortex uses intracortical long-range projections to mediate interactions across visual space. These lateral connections provide contextual modulation of the receptive field (Das and Gilbert, 1999; Series et al., 2003) and allow us to process a much wider range of component images.

One of the most common forms of contextual modulation within V1 is suppression when a stimulus exceeds the optimal size (Liu et al., 2011; Jones et al., 2001; Sengpiel et al., 1997; Walker et al., 2000). Inhibitory neurons play a key role in this size tuning. About 20% of the cells in visual cortex are GABAergic and inhibit the neural signal when the stimulus exceeds the optimal size of the cell. These inhibitory neurons are local only and are thought to be driven by inputs from long-range projections which are typically excitatory in nature (Hirsch and Gilbert, 1991; Ahmed et al., 1994; Anderson et al., 1994; Weliky et al., 1995). Excitation of these inhibitory cell bodies changes the response to a stimulus based on its' presentation; in this way, the primary visual cortex begins the distinction from one stimulus to another.

There are several subtypes of inhibitory neurons found in the visual cortex. Parvalbumin (PV), calbindin (CB), and calretinin (CR) neurons comprise 95% of the inhibitory neuron

population in macaque V1 (Disney and Aoki, 2008). PV neurons comprise the majority of these three, about 74% of GABAergic neurons (Van Brederode et al., 1990). Disney et al. (2008) found that 87% of PV-immunoreactive neurons in macaque V1 expressed m1 AChRs, suggesting that the role of acetylcholine release in V1 is primarily targeting PV neurons and may function to modulate network-level spike synchronization.

Functional Implications of Cholinergic Modulation in V1:

Given the evidence for cholinergic targeting of inhibitory neurons in V1 and the role of inhibitory neurons in visual processing, we can make certain predictions regarding the purpose of this projection pathway. It is likely that the projection plays a role in modulating a neuron's preferential stimulus size, given the role of surround/suppression in V1. Indeed, when recording electrical activity of V1 neurons following extracellular iontophoretic application of acetylcholine, Roberts et al. (2005) noted a shift in the neuron's preferred stimulus length towards shorter bars (See figure 0.3). This led to the conclusion that acetylcholine plays a direct role in controlling spatial integration (Roberts et al., 2005) and supports the idea that cholinergic modulation reduces the response of neurons to inputs further apart in V1 due to presynaptic inhibition of intracortical excitatory synapses (Disney et al., 2006; Disney and Aoki, 2008). These results were later shown in human visual cortex. Silver et al. (2008) administered acetylcholinesterase blockers to human subjects during an fMRI study. Results confirmed a reduction of retinotopic spread in response to visual stimuli (Silver et al., 2008; Newman et al., 2012).

Additionally, acetylcholine has been shown to be vital in a V1 neurons' ability to change firing rate based on a learned prediction of reward (Shuler and Bear, 2006). Through the course

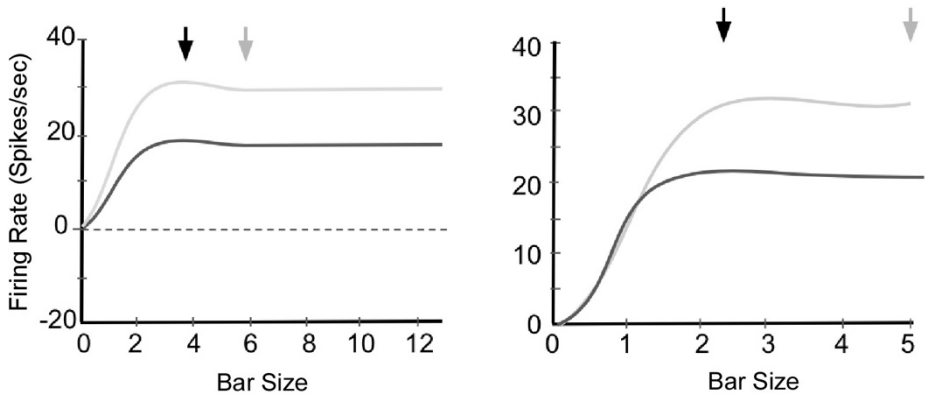

Figure 0.3: Example of firing rates from two cells in V1 during stimulus presentation following application of acetylcholine (black lines) and without acetylcholine (grey lines). Smooth lines show fitted differences of Gaussian models. Arrows above each graph indicate the peak of the fitted curve and represent the preferred length. Both examples indicate a shift towards a smaller bar size preference. Based on results from Roberts et al., 2005.

of conditioning, V1 neural responses evolve from relating simple features of the visual cues to expressing what these cues have come to predict: the expected time of reward (Shuler and Bear, 2006). Rapidly predicting the identity and timing of new events is critical for survival, allowing animals to exploit resources and avoid harmful situations. Chubykin et al. (2013) demonstrated that the cholinergic basal forebrain projection neurons are necessary for this learning outcome. Using a delay-reward conditioning task, animals were trained to predict a desired outcome with either of two visual cues. After demonstrated learning of the task, animals were injected with 192-IgG-saporin into the recording site in V1, which eliminates only cholinergic basal forebrain inputs into the infusion zone. Following the injection, the animals lost the ability to update cue-reward intervals, maintaining only those that were learned prior to infusion. This indicates that cholinergic release in V1 plays a critical role in learning reward timing activity, and specifically the basal forebrain cholinergic input is necessary for this plasticity to occur.

These studies have demonstrated pharmacological application of cholinergic agonists and antagonists. With the advent of transgenic capabilities in mice, we can now directly manipulate a cortical pathway in vivo. Manipulation of cholinergic input to V1 has been shown to directly

alter visual perception and indicates an important role in sensory processing. Pinto et al. (2013) observed perceptual changes when directly modulating the pathway via optogenetic manipulation, which utilizes photosensitive cell membrane channels to either enhance or inhibit normal cell responses. A channelrhodopsin (ChR) genetic tag activates the function of the tagged neuron when it is stimulated by blue light. In contrast, a halorhodopsin or archaerhodopsin tag will mute the effects of the targeted pathway (Han and Boyden, 2007; Zhang et al., 2007; Osakada et al., 2011) when activated with yellow light. Using transgenic mice expressing ChR2-modulated choline acetyltransferase, Pinto et al. (2013) noted increased firing rates and enhanced visual perception when firing a laser through an implanted optic fiber in the basal forebrain. Mice that were trained on a go/no-go task to discriminate between vertical and horizontal drift gratings showed improved performance when the basal forebrain cholinergic neurons were activated. Additionally, inactivation in expressing HALO in cholinergic neurons showed decreased behavioral performance on the same task. These behavioral results suggest that the basal forebrain activation improves sensory processing in V1 via increased spontaneous and visually driven cortical firing rates and improved neuronal response reliability.

The effects of cholinergic activation described above- improved neuronal response reliability and increased spontaneous and visually driven cortical firing rates- have also been observed during selective visual attention tasks (Pinto et al, 2013; Reynolds et al., 2000; Williford & Maunsell, 2006). This similarity strongly suggests that cholinergic transmission is likely to be a key component of the neural mechanism for attention modulation (Pinto et al, 2013). In a study completed by Herrero et al. (2008), cholinergic antagonists were used to during an attention task to see the direct relationship between acetylcholine and attention. Recordings from V1 showed a reduction in attentional modulation (as measured by analyzing the receiver

operating characteristic curve on the basis of single trial responses) following administration of the muscarinic antagonist scopolamine. Notably, the nicotinic antagonist mecamylamine had no systematic effect. These results demonstrate that muscarinic cholinergic mechanisms play a central part in mediating the effects of attention in V1. While both nicotinic and muscarinic receptors are present on inhibitory and excitatory neurons in V1, this work shows that it is primarily the muscarinic receptor that contributes to attentional modulation. Furthermore, because the majority of neurons having muscarinic receptors are inhibitory in V1 (Disney et al., 2006), the net effect of attention is likely to be inhibitory.

These studies have led to proposals suggesting the functional role of acetylcholinergic release in V1 is to restrict information flow to subsequent higher visual areas. This would filter the information based on receptive field size and focus the target area for more detailed information processing. Once the information is passed on to higher visual areas, cholinergic modulation takes a different form and serves more of an excitatory role to enhance firing (cite all the relevant studies again here, not including the two below). This is supported by neurophysiological evidence showing that attentional tasks increase firing rates of neurons in higher visual areas such as monkey V4, but not significantly in V1 (McAdams and Maunsell, 1999). Anatomical evidence from V2 also supports this shift in functionality. Disney et al. (2006) found that 63% of V2 cells with the m1 receptor and 65% with the m2 receptor were excitatory, whereas the percent of excitatory cells in V1 was less than 50% for either receptor. Therefore, higher area V2 excitatory neurons are more susceptible to cholinergic modulation than V1 excitatory neurons.

Role of Attentional Modulation in V1:

As described above, the cholinergic projection pathways are implicated in the inhibitory mechanisms of visual processing in V1. The purpose for the modulation is thought to be tied to effects of attention (Herrero et al., 2008; Spitzer et al., 1988; Treue et al., 1996). Attention has been shown to increase firing rates and affect tuning properties in visual cortex (Herrero et al., 2008; Spitzer et al., 1988; Treue et al., 1996; Reynolds et al., 1999; Roelfsema et al., 1998; Roberts et al., 2007). There are several theories of attention that correspond with these functional results.

One model of attentional modulation through cholinergic interactions suggests there is a combined effect of decorrelation and increased response reliability mediated through activation of the nucleus basalis of the basal forebrain (Thiele, 2009; Goard & Dan, 2009). This theory posits that the release of acetylcholine from the nucleus basalis onto mAChRs on lateral connections from local cortical interneurons causes reduced crosstalk between these cortical neurons and affects their correlation, reducing redundancy of information processing. Additionally, this theory suggests that the nucleus basalis projections to the reticular thalamic nucleus promotes the flow of information from the sensory periphery to the cortex by disinhibiting neurons in the relay nucleus, resulting in increased response reliability (Thiele, 2009; Goard & Dan, 2009). This theory is consistent with evidence showing that blocking mAChRs blocks attention modulation in V1 (Herrero et al., 2008). This work suggests that during states of arousal and attention, the basal forebrain neuromodulatory circuit acts on local and distributed mechanisms to improve sensory coding (Goard & Dan, 2009).

A second model, the normalization model of attention, has been posed to account for the various effects on the responses of neurons in V1 with different attention protocols (Reynolds & Heeger, 2009). This model combines three basic components of a visual stimulus: the region in

the cell's preferred receptive field (the "stimulation field"), the region that is suppressed in the receptive field (the "suppressive field"), and the region that is being attended to (the "attention field"). The stimulation field is the baseline for the cell, while the suppressive field is divisive so that the baseline for a preferred stimulus is normalized with respect to the activity in other neurons that respond to the surrounding context. The attention field is compounded with the stimulus drive from the stimulation field before normalization, therefore causing an effect on the cell's firing rate due to its influence on both the stimulation field and suppressive field. In this normalization model of attention, attention causes a shift in the distribution of activity across the population of neurons, either via excitation or inhibition.

Both models provide a possible understanding of how attention towards a stimulus can cause a direct impact on the tuning of V1 cells. Through the use of neuroanatomical analysis, perhaps we can shed light as to which model is more likely to be employed through the specific projection from BF cholinergic neurons.

Current Methods and Analysis:

Numerous methods have been used to identify projection neurons and illuminate their role in neural processing. One such method utilizes the diverse network of neurotransmitters in the brain to highlight the specific nature of projection patterns and their potential functional roles. This recently-developed technique uses a helper virus containing a specific promoter to target a genetically modified rabies virus for retrograde tracing of the direct inputs to either inhibitory or excitatory V1 neurons. In chapter 1, we use this tracing method with non-selective glycoprotein-deleted (ΔG) rabies virus to confirm the presence of this projection and narrow down the specific input and output regions; ΔG rabies virus acts as a highly efficient retrograde

tracer. Then, using helper viruses with cell type specific promoters to target retrograde infection of pseudotyped and genetically modified rabies virus, we found evidence for direct synaptic input onto V1 inhibitory neurons. These inputs were similar in number to geniculocortical inputs, and, therefore, considered robust. In contrast, while clear evidence for dorsal lateral geniculate nucleus input to V1 excitatory neurons was found, there was no evidence of direct synaptic input form the basal forebrain, only indirectly onto excitatory neurons through diffuse transmission. This inhibitory neuron specific circuit suggests a greater role of the basal forebrain in suppression of V1 neuron responses.

While no direct inputs to excitatory neurons were found, these previous results were achieved using a less effective rabies glycoprotein (B19 strain) for trans-complementation. One possibility is that excitatory neurons do receive direct basal forebrain inputs, but to a lesser degree than inhibitory neurons, and that the tracing method previously used was not sufficiently sensitive. In Chapter 2, we utilized a new optimized rabies glycoprotein (oG) reported to be 10 times more effective in labeling presynaptically connected neurons. With oG we found an overall improvement in tracing of inputs to both inhibitory and excitatory neurons compared to the B19 strain of glycoprotein. An increase of more than 10 times as many LGN inputs to V1 excitatory neurons were found. Nevertheless, an average of only 1 basal forebrain neuron per case was found to project to excitatory neurons. These results are largely consistent with the previous findings, confirming that even with enhanced viral infection, excitatory neurons do not receive a significant direct input from the basal forebrain.

Finally, we wanted to understand the functional implications of this predominantly cholinergic input to V1. At the neuronal level, demonstrated effects of external application of acetylcholine in V1 range widely from cell to cell; for example some cells increase firing rate,

while others show a decrease in response to optimal visual stimuli. Part of this diversity may be due to differences between direct synaptic contact of basal forebrain inputs which primarily target deep layer inhibitory neurons versus diffuse transmission of acetylcholine which targets excitatory neurons and inhibitory neurons in superficial cortical layers. To address this, our study utilized a retrograde-tracing method to deliver light-gated ion channels to basal forebrain projection neurons, allowing for direct optogenetic manipulation during single unit recording in V1 of anesthetized rats. In doing so, we found significant suppression of cell response to the preferred stimulus with basal forebrain activation. Conversely, we found that responses to stimuli smaller than the optimal size were facilitated during basal forebrain activation. Thus, basal forebrain effects on V1 neurons depend on stimulus size. Neurons in the 4 cases are analyzed and a total of 31 cells collected to demonstrate an effect on preferred stimulus size. We examine the differences among cortical layers to further distinguish the role acetylcholine plays in the cortex and provide insight into the mechanism of cholinergic modulation from visual processing.

CHAPTER 1: CELL TYPE SPECIFIC TRACING OF THE SUBCORTICAL INPUT TO PRIMARY VISUAL CORTEX FROM THE BASAL FOREBRAIN.

Visual perception occurs through a complex network of cortical processing that relies on driving, modulating, and integrating interconnectivity with subcortical visual structures, as studied extensively in rodents (Guillery & Sherman, 2002; Krubitzer, Campi, & Cooke, 2011; Marshel, Garrett, Nauhaus, & Callaway, 2011; Niell, 2015; Negwer, Liu, Schubert, & Lyon, 2017; Seabrook, Burbridge, Crair, & Huberman, 2017), carnivores (Reid & Alonso, 1995; Liu, Hashemi- Nezhad, & Lyon, 2011; Hashemi-Nezhad & Lyon, 2012), non-human primates (Felleman & Van Essen, 1991; Casagrande, 1994; Lyon et al., 2002; Casagrande, Sary, Royal, & Ruiz, 2005; Kaas, 2012), and close relatives such as the tree shrew (Casagrande & Harting, 1975; Lyon, Jain, & Kaas, 1998; Casagrande, Xu, & Sary, 2002). The lateral geniculate nucleus (LGN), the superior colliculus, and the pulvinar nucleus are among the most studied subcortical visual regions, having been subject to decades of anatomical and functional investigation by Vivien Casagrande and her colleagues in tree shrew (Casagrande, Harting, Hall, Diamond & Martin, 1972; Lyon, Jain, & Kaas, 2003a, b; Vanni, Thomas, Petry, Bickford, & Casanova, 2015) and primate (Fitzpatrick, Carey, & Diamond, 1980; Lachica & Casagrande, 1992; Stepniewska & Kaas, 1997; Xu et al., 2001; Nassi, Lyon, & Callaway, 2006; Imura & Rockland, 2006; Kaas & Lyon, 2007; Lyon, Nassi, & Callaway, 2010; Purushothaman, Marion, Li, & Casagrande, 2012; Cerkevich, Lyon, Balaram, & Kaas, 2014), and by many others in rodent (Lysakowski, Standage, & Benevento, 1986; Sanderson, Dreher, & Gayer, 1991; Van Hooser & Nelson, 2006; Marshel, Kaye, Nauhaus, & Callaway, 2012; Cruz-Martín et al., 2014; Tohmi, Meguro, Tsukano, Hishida, & Shibuki, 2014; Roth et al., 2016; Seabrook et al., 2017; Zhou,

Maire, Masterson, & Bickford, 2017; Zhou, Masterson, Damron, Guido, & Bickford, 2018). The basal forebrain has also been known to provide input to the visual cortex (Henderson, 1981; Tigges et al., 1982; Carey & Reick, 1987; Dreher, Dehay, & Bullier, 1990), yet it's functional contribution is only starting to become understood (Goard & Dan, 2009; Newman, Gupta, Climer, Monaghan, & Hasselmo, 2012; Pinto et al 2013). The basal forebrain output to cortex is predominantly characterized as cholinergic (Henderson, 1981; Sarter, Hasselmo, Bruno, & Givens, 2005; Pinto et al., 2013). Given the high density of cholinergic varicosities within V1 (Lysakowski et al., 1989; Mechawar et al., 2000) and the functional contribution of acetylcholine to plasticity in V1 (Bear and Singer, 1986), acetylcholine from the basal forebrain is particularly well suited to reinforce V1 (Chubykin et al., 2013).

Acetylcholine from the basal forebrain is delivered to V1 across most cortical layers via diffuse extra-synaptic modulation known as 'volume transmission' (Descarries, Gisiger, & Steriade, 1997; Sarter et al., 2005). This is reinforced by anatomical evidence showing acetylcholine receptors evenly distributed across layers 2-6 (Disney, Domakonda, & Aoki, 2006; Disney & Reynolds, 2014). In layers 2/3, 5, and 6, cholinergic receptors are found predominantly on inhibitory neurons leading to GABAergic mediated suppression (Disney et al., 2006; Disney, Aoki, & Hawken, 2007; Disney, Aoki, & Hawken, 2012; Disney & Reynolds, 2014). Furthermore, basal forebrain afferents terminate exclusively within infragranular layers 5 and 6 (Carey & Rieck, 1987; Rieck & Carey, 1984). Therefore, unlike superficial cortical layers, the effect on neurons in layers 5 and 6 can be more immediate.

Based on the preponderance of cholinergic receptors being found on inhibitory neurons (Disney et al., 2016, Disney & Reynolds, 2014), one might expect direct synaptic basal forebrain inputs to primarily contact inhibitory neurons. To determine this, we took advantage of our

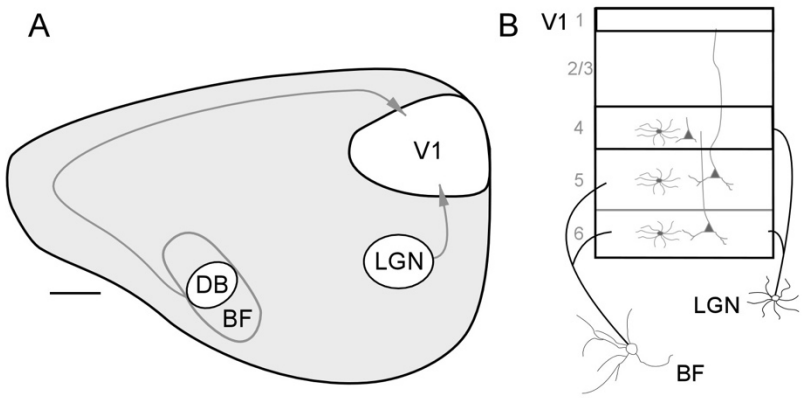

Figure 1.1 Schematic of basal forebrain projection to mouse V1. (A) The basal forebrain (BF) projects to V1 from neurons located in the diagonal band (DB) region. V1 input from the lateral geniculate nucleus (LGN) of the thalamus is also indicated. Scale bar equals 1mm. (B) Basal forebrain inputs terminate in layers 5 and 6; LGN inputs terminate primarily in layers 4 and 6.

recently developed technique (Liu et al., 2013), where a helper virus containing either a GAD1 or an αCamKII promoter is used to target a genetically modified rabies virus (Wickersham et al., 2007) for retrograde tracing of the direct inputs to either inhibitory or excitatory V1 neurons, respectively. In this way, we are able to determine whether or not there is a difference in direct synaptic inputs of the basal forebrain to inhibitory and excitatory neurons.

1.1 Materials and methods:

Eighteen adult C57BL/6 mice of both sexes were used following procedures approved by the University of California, Irvine Institutional Animal Care and Use Committee and the Institutional Biosafety Committee, and the guidelines of the National Institutes of Health were followed.

Six mice were given 9 injections of the mCherry (mCh) and/or green fluorescent protein (GFP) versions of the glycoprotein-deleted rabies virus (ΔG-RV; Table 1). Twelve different mice were given injections of a helper virus (AAV-GAD1-YTB or LV-αCamKII-YTB; Table 2). Anesthesia was induced and maintained with isofluorane throughout the procedure. Once

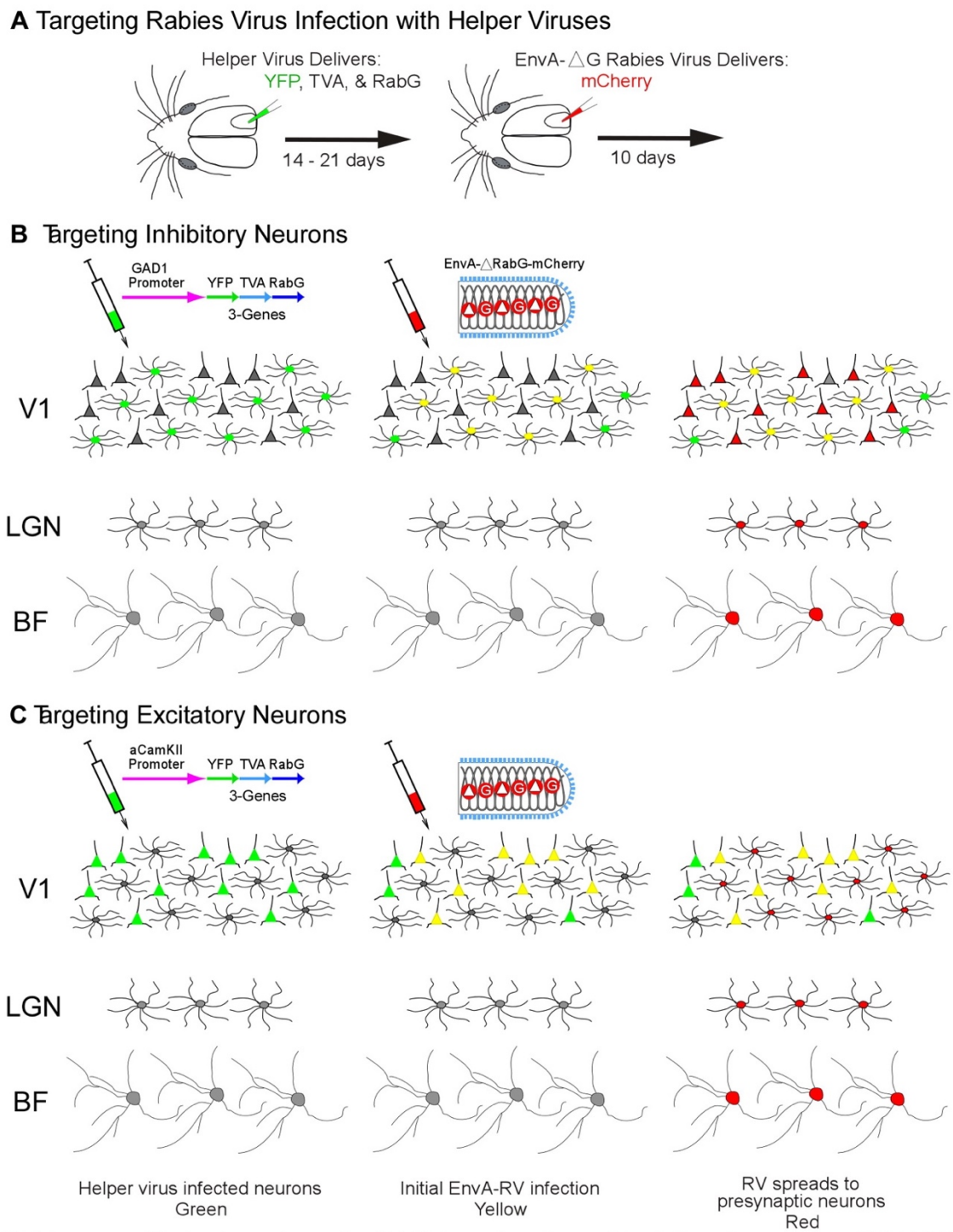

Figure 1.2 Cell type specific tracing schematic. (A) Helper virus is used to deliver three genes (YFP, TVA, RabG) to a local population of neurons in mouse V1 (left). Following a 2-3 weeks survival period, EnvA-△G-RV which will express mCherry in infected neurons is injected into the same V1 location (right). The RV injection is followed by a 10 day survival period. (B,C) (Left) Helper virus cell type specificity is achieved with the GAD1 (a) or aCamKII(c) promoter. In this way the YFP reporter (green) will express only the V1 inhibitory (b) or excitatory pyramidal (c) neurons. (Middle) EnvA-△G-RV can only infect neurons expressing the TVA receptor, the second gene product of the helper virus. Resulting super-infected neurons are identified by co-expression of YFP and mCherry (yellow). (Right) Expression of the RabG, the third helper virus gene product, is incorporated into the △G-RV-mCherry produced within super-infected neurons (starter cells; yellow) enabling RV to infect presynaptically connected neurons (red).

anesthetized, animals were placed in a stereotaxic head-holder and craniotomy was performed

over the caudal half of the neocortex under sterile conditions. Glass pipettes with tips broken to approximately 20 μm were filled with virus and inserted through dura using a computer-controlled micro-positioner attached to a KOPF stereotaxic arm. Coordinates between 3.0 and 4.5mm posterior from Bregma and 1.25-3.25mm lateral to the midline were used. ΔG-RV injections were made at a depth of ~500μm and a volume of ~0.3μl.

For AAV and LV helper viruses, ~0.5μl injections were made in a single V1 location at a cortical depth between 400 and 600μm. After injection, artificial dura (Tecoflex, Microspec Corp.) was placed over the craniotomy, the skull sealed with dental acrylic, and the animals revived. Mice injected with ΔG-RV were given a 7-10 day survival time and then perfused for histology.

Mice injected with helper virus were given a 3-week survival period followed by an intracranial injection of EnvA-ΔG-RV (see Figure 1.2 for injection timelines). For EnvA-ΔG-RV injections, each animal was anesthetized as before, and under sterile conditions the acrylic skull cap removed and EnvA injections of ~0.5μl made as close as possible to the original helper virus injected location based on the coordinates and landmarks described above. The craniotomy was then covered with fresh Tecoflex, resealed with dental acrylic, and the animals revived. A final survival period ranging from 7 to 10 days followed.

1.1a Viruses:

The ΔG-RV expressing either mCherry or GFP, and the EnvA-ΔG-RV expressing mCherry were produced and concentrated following protocols described previously (Wickersham et al., 2007; Wickersham, Sullivan, & Seung, 2010; Osakada & Callaway, 2013) with a titer range of ~$5x10^9$ infectious units/ml.

For helper viruses, GAD1-YTB (7,382bp) and αCamKII-YTB (7,500bp) were sub cloned into adeno-associated virus (AAV) and lentiviral (LV) backbones to make AAV-GAD1-YTB (11.0kb) and LV-αCamKII-YTB (12.3kb), as described previously (Liu et al., 2013). From these plasmids, serotype 9 AAV and VSV-G pseudotyped LV particles were prepared and purified by the Gene Transfer Targeting and Therapeutics Core at the Salk Institute of Biological Studies (La Jolla, CA) yielding a titer of $9x10^9$ genome copies/mL for AAV and $2x10^{10}$ transducing units/ml for LV.

1.1b Histology and antibody reporting:

For histology, animals were deeply anesthetized with Euthasol and perfused transcardially, first with saline, then followed by 4% paraformaldehyde in phosphate buffer (PB; pH 7.4). For most animals, 1.5% glutaraldehyde was also included. Brains were removed and cryoprotected in 30% sucrose for ~48hr prior to sectioning.

Brains were cut coronally at 30µm up to 1mm posterior and anterior to the V1 injection site, and at 40µm thickness elsewhere. A series of every fourth 30µm section was processed for GABA using the anti-GABA rabbit polyclonal antibody (1:200; Sigma-Aldrich Cat #A2052, RRID:AB477652; tested in GABA expressing cells isolated from the pallidum in mice; conjugated to BSA). Immunopositive neurons were revealed using fluorescent secondary Alexa Fluor 350 goat anti-rabbit IgG (1:500; Invitrogen). To enhance visualization of yellow fluorescent protein (YFP) the same sections were also processed for the anti-GFP chicken polyclonal antibody (1:1000, Novus Cat#NB100-1614, RRID:AB523902; tested on transgenic mice expressing recombinant GFP: Immunogen affinity purified) and revealed using Alexa Fluor 488 goat anti-chicken IgG (1:500; Invitrogen). The mCherry and GFP reporters from rabies virus

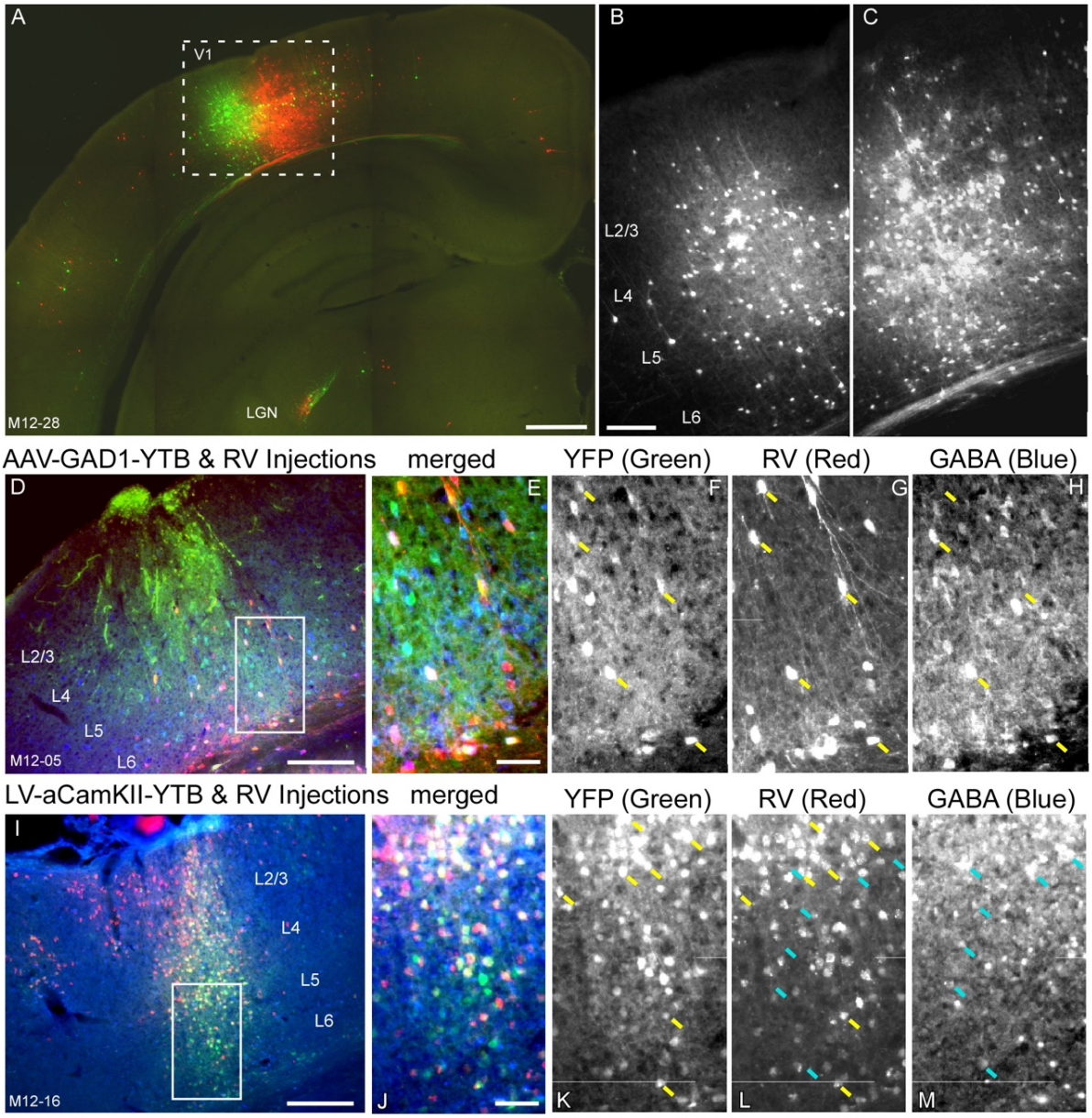

Figure 1.3: Digital images of virus injection sites in V1. (A) Injections of △G-GFP (green) and △G-mcherry (red) are shown side-by side in case M12-28. (B,C) Higher magnification digital images of the same GFP (b) and mCherry (c) △G-RV are shown in black and white and indicate that injection sites extended through layers 4-6. (D) Injection sites of AAV-GAD1-YTB expressing YFP (green) and EnvA- △G-RV expressing mCherry (red) are shown in a section through V1 processed for the GABA antibody (blue) in case M12-05. (E-H) Higher magnification images of the layer 5/6 region outlined by the white rectangle in (D). Inhibitory starter cells co-expressing YFP (F) and mCherry (G) are positive for the GABA antibody (h); for reference a portion of starter cells are identified by yellow markers. (I) Injection sites of LV-aCamKII-YTB expressing YFP (green) and EnvA-△G-RV expressing mCherry (red) are shown in a section through V1 processed for the GABA starter cells co-expressing YFP (K) and mCherry (L) are negative for the GABA antibody (H); a sample of starter cells are identified by yellow markers; a sample of GABA-positive neurons are marked by blue markers. Scale bar in (A,D, I) equal 200um; Scale bars in (B, E, J) equal 50um.

were not enhanced through immunofluorescence. One to two additional series of every fourth section were processed instead for DAPI. Rabies virus infected neurons could be visualized in all sections without processing. Sections were cover-slipped in PVA-DABCO (Sigma-Aldrich) to preserve fluorescence.

1.1c Data analysis:

Sections were examined using fluorescent microscopy (Zeiss Axioplan) with 10x (0.45NA) and 20x (0.8NA) objectives and cell positions reconstructed using Neurolucida software (MicroBrightField, Willston, VT) offline. To limit bleaching of fluorescence, images of whole sections were captured with high-power black and white digital camera (Cooke SensiCam QE) and stitched together through the Virtual Slide module.

For each case, two or three of every four sections were used to identify the number and laminar location of starter cells in V1 and rabies infected neurons in the dorsal lateral geniculate nucleus and diagonal band of the basal forebrain. Interpolated cell-counts were generated for Tables 1 and 2 by multiplying the number of cells by two for cases where two out of four sections were examined, or multiplying by 1.33 for cases where three out of every four sections were used.

Confirmation of V1 injection sites and the locations of the LGN and diagonal band were based on the atlas by Paxinos and Franklin (2001).

1.2 Results:

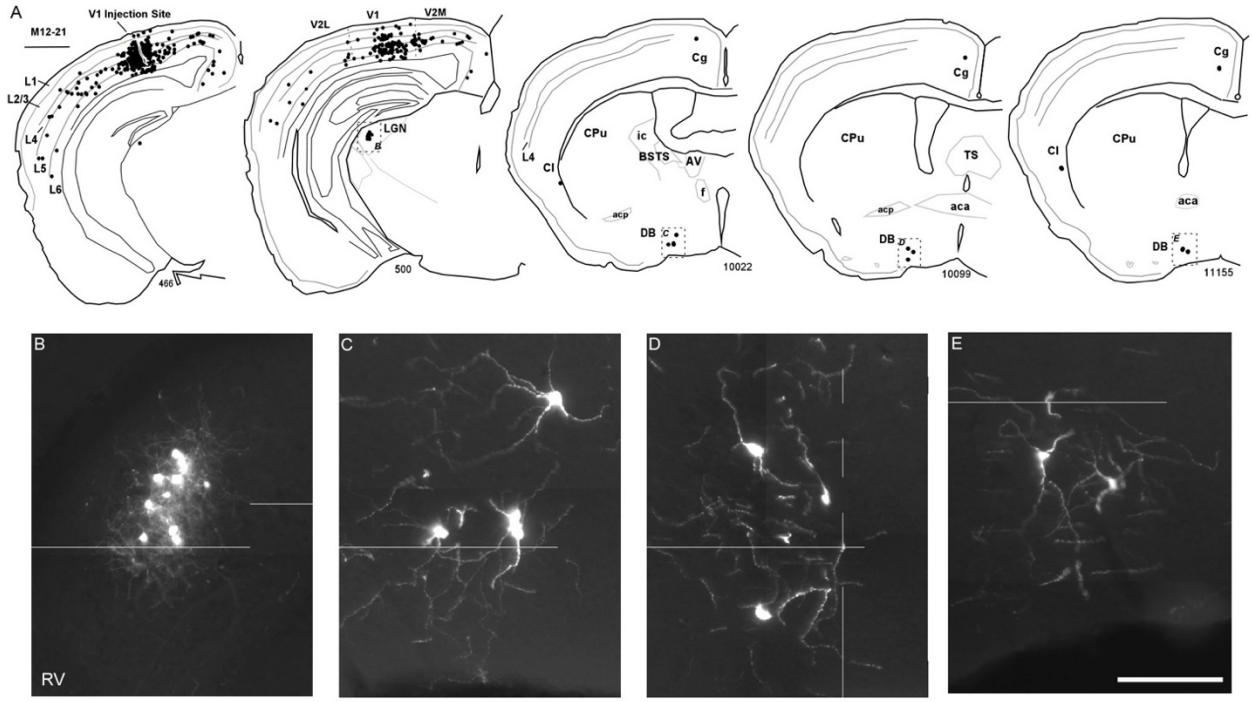

Figure **1.4** Retrogradely infected neurons in the diagonal band of the basal forebrain following V1 injection of△G-RV. (A) A reconstruction of the pattern of rabies virus infected neurons (black dots) in 5 coronal sections presented from posterior (section 46) to anterior (section 115) in case M12-21. The V1 injection site is shown in section 46. Scale bars equal 1mm. (B-E) Digital Images of rabies virus infected neurons in the LGN (B) and diagonal band of the basal forebrain (C-E) from regions corresponding to dashed rectangles in (B). Scale bars equal 200um.

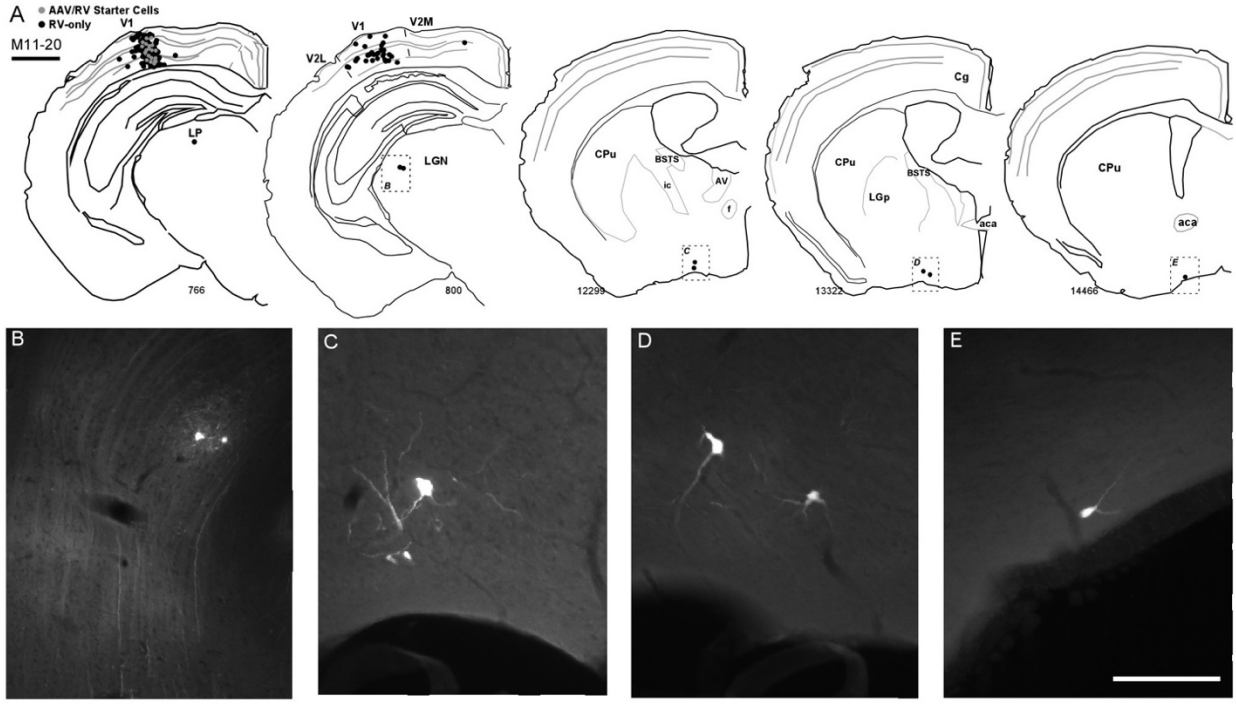

Figure **1.5** Basal forebrain neurons project directly to V1 inhibitory neurons. (A) V1 inhibitory starter cells (grey dots) shown at the injection site in section 76, resulted from injection of AAV-GAD-YTB followed three weeks later by injection with EnvA△G-RV (see figure 2.2A,B). Presynaptic inputs to inhibitory starter cells are also shown (black dots). (B-E) Digital images of rabies virus infected neurons in the LGN (B) and diagonal band of the basal forebrain (C-E) from regions outlined by dashed rectangles in (A). Other conventions are as in Figure 4.

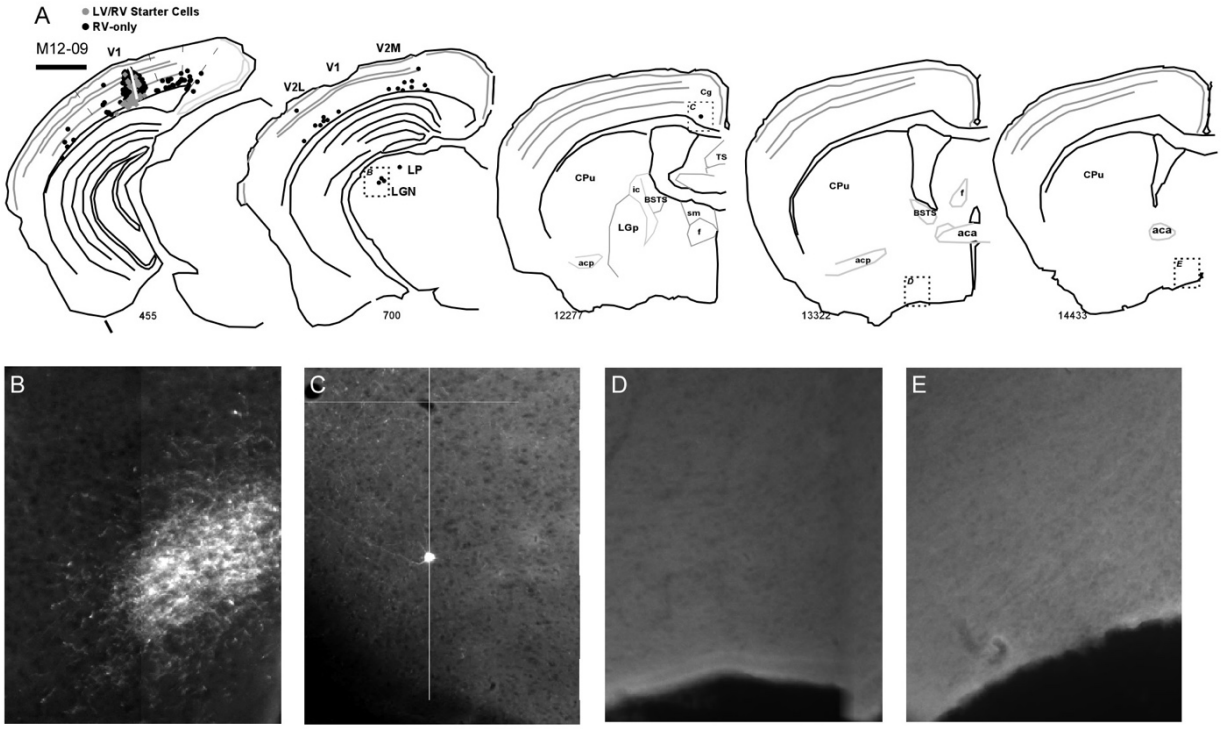

Figure 1.6: No evidence for direct basal forebrain inputs to V1 excitatory neurons. (A) Excitatory starter cells (grey dots) shown at the injection site in section 45, resulted from injection of LV-aCamKII-YTB followed three weeks later by injection with EnvA-△G-RV (See figure 1.2A,C) Presynaptic inputs to excitatory starter cells are also shown (black dots). Scale bar equals 1mm. (B-E) Digital images of the regions outlined in (A). Rabies virus infected neurons were found in the LGN and cingulate cortex, but not in the basal forebrain (D,E). Other conventions are as in Figure 4.

Using injections of cell type specific viral tracers in V1, we found that neurons in the basal forebrain project directly to V1 inhibitory neurons, but found no evidence for direct projections to cortical excitatory neurons. We also found the basal cortical projections to be similar in number of LGN inputs to V1.

1.2a ΔG-RV retrograde infection of basal forebrain

Prior to using the cell type specific helper viruses to target EnvA-ΔG-RV, we first made injections of ΔG-RV. The ΔG-RV version of rabies virus acts as a monosynaptic retrograde tracer and does not require a helper virus (Wickersham et al., 2007; Connolly, Hashemi-Nezhad,

& Lyon, 2012). While this virus cannot distinguish between inputs to inhibitory and excitatory neurons, the goal of these injections was to determine the ability and degree to which rabies virus infects basal forebrain neurons targeting V1 by comparing the number of infected neurons in LGN.

Nine distinct injections of ΔG-Rabies virus with either the mCherry or GFP promoter were made into V1 of 6 mice (Table 1). All 9 injections resulted in labeled neurons in the diagonal band of the basal forebrain and the LGN, with the average number for basal forebrain (13.4 +/- 4.9) about two thirds that of the number of neurons found in the LGN (21.3 +/- 6.5).

An example of two injections in the same animal is shown in figure 1.3a. Based on the density of intrinsic V1 labeled neurons, the injection sites reached layers 4, 5, and 6 which would be necessary to target axon terminals from LGN and basal forebrain neurons. A reconstruction of the pattern of labeled cells from an injection in a second case is shown in Figure 1.4a. The reconstruction of posterior sections 45 and 50 shows that the V1 injection site extended through layers 4, 5, and 6. Expected inter-areal connections with other visual cortical areas were observed, along with a cluster of neurons in the LGN. In more anterior sections (102, 109, 115) clusters of basal forebrain neurons are shown ventral medially, along with a few labeled neurons in cingulate cortex dorsal medially, and the claustrum laterally. Digital images show that labeled diagonal band neurons had a distinct large soma size and long spiny dendrites (figure 1.4c,d). Compared to basal forebrain neurons, LGN neurons were packed together more tightly

Table 1.1: Number of Retrogradely Infected Neurons in the Diagonal Band and LGN following glycoprotein deleted rabies virus injections in mouse V1.

Case No.	Rabies Virus	Diagonal Band	LGN
M12-13	ΔG-GFP	2	3
M12-13	ΔG-mCh	3	3
M12-21	ΔG-mCh	51	52
M12-22	ΔG-mCh	8	16
M12-27	ΔG-mCh	6	6
M12-28	ΔG-GFP	11	42
M12-28	ΔG-mCh	14	45
M12-29	ΔG-GFP	14	10
M12-29	ΔG-mCh	12	15

with smaller somas and shorter dendrites (4b).

1.2b AAV-GAD-YTB targeted retrograde tracing with EnvA-ΔG-RV

To determine whether basal forebrain neurons project to V1 inhibitory neurons, we made injections of the helper virus AAV-GAD1-YTB, to target infection of the retrograde EnvA-ΔG-RV to inhibitory neurons. Injections were made into a single V1 hemisphere of 6 mice (Table 1.2). In five of six cases, retrograde infected neurons were found in the diagonal band of the basal forebrain, averaging 8 +/- 3.4 per case. Five cases also yielded labeled neurons in the LGN with an average number of 13 +/- 5.1 (Lean et al., 2019).

An injection site example is shown from one case in Figure 1.3d-h. YFP-expressing neurons (Figure 1.3f) were confirmed as inhibitory through co-labeling with the GABA-antibody (figure 1.3h). Rabies virus infected neurons expressed mCherry. Starter cells in V1 were defined as neurons co-expressing YFP and mCherry (yellow neurons in figure 1.3e); neurons expressing mCherry only were defined as presynaptically connected neurons. Starter cells were evident throughout layers 4, 5, and 6 (see table 1.2).

A reconstruction of the distribution of inputs to V1 inhibitory starter cells is shown in a second case (Figure 1.5a). Starter cells were distributed throughout all layers as shown in section 76, with presynaptically connected neurons found in the LGN in section 80 (Figure 1.5b) and in the diagonal band of the basal forebrain (Figure 1.5c-e) as shown in the three most anterior sections. Overall, a nearly equal number of starter cells were present in layer 5 and 6, and a nearly equal number of presynaptic neurons were labeled in the diagonal band and LGN (Table 1.2).

1.2c LV-αCamKII-YTB targeted retrograde tracing with EnvA-ΔG-RV

To determine whether the basal forebrain neurons project to V1 excitatory neurons, we made injections for the lentiviral vector, LV-αCamKII-YTB, to target infection of the retrograde EnvA-ΔG-RV to excitatory neurons. Injections were made into a single V1 hemisphere of 6 mice (see table). In five of six cases, retrograde infected neurons were found in the LGN (6.4+/- 1.7 per case). However, no infected neurons were found in the basal forebrain.

An injection site example is shown from one case in Figure 1.3i-m. YFP expressing neurons (Figure 1.3k) were confirmed as excitatory for not co-labeling with the GABA antibody (Figure 1.3m). Rabies virus infected neurons expressed mCherry (Figure 1.3l). Starter cells in V1 were defined as neurons co-expressing YFP and mCherry (yellow neurons in Figure 1.3j); Neurons expressing mCherry only were defined as presynaptically connected neurons. Yellow starter cells were evident throughout layers 4, 5, and 6 (Figure 1.3j; see also Table 1.2).

A reconstruction of the distribution of inputs to V1 excitatory starter cells is shown in a

Table 1.2: Number of retrogradely infected neurons in the diagonal band and LGN projecting to V1 starter cells in Layers 4, 5, and 6

Case No.	Helper Virus	Starter Cell Type	Starters No.: Layer 4	Layer 5	Layer 6	Diagonal Band	LGN
M11-16	AAV-GAD1	Inhibitory	35	3	1	0	16
M11-20	AAV-GAD1	Inhibitory	3	14	13	23	22
M12-05	AAV-GAD1	Inhibitory	7	22	34	6	2
M12-06	AAV-GAD1	Inhibitory	4	17	39	13	7
M12-07	AAV-GAD1	Inhibitory	6	42	28	2	0
M12-17	AAV-GAD1	Inhibitory	9	44	24	4	32
M11-19	LV-αCamKII	Excitatory	6	16	22	0	4
M12-09	LV-αCamKII	Excitatory	3	48	38	0	8
M12-10	LV-αCamKII	Excitatory	2	12	26	0	0
M12-15	LV-αCamKII	Excitatory	32	53	60	0	12
M12-16	LV-αCamKII	Excitatory	13	16	13	0	4
M12-26	LV-αCamKII	Excitatory	8	11	4	0	4

second case (Figure 1.6a). In the posterior most section, starter cells were distributed throughout layers 4, 5, and 6, with presynaptically-connected neurons found in the LGN in section 70 (Figure 1.6b). Presynaptically-infected neurons were labeled as far posterior as the cingulate cortex (Cg), but no cells were found in the basal forebrain.

1.3 Discussion

The goal of this present experiment was to determine the cell type specific nature of projections from the basal forebrain to primary visual cortex. Using a dual viral retrograde tracing method, we found evidence for direct synaptic input to inhibitory neurons (Figure 1.7). These inputs were robust as they were similar in number to geniculocortical inputs to inhibitory neurons (Table 1.2). In contrast, we found clear evidence for LGN input to V1 excitatory neurons, but no evidence for direct synaptic input from the basal forebrain (Figure 1.7). Taken

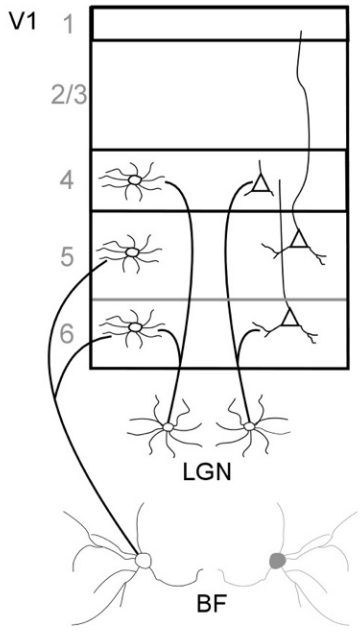

Figure 1.7: Summary of cell type specific basal forebrain input to V1. Based on the results from our dual viral tracing method, V1 inhibitory neurons receive direct inputs from the basal forebrain and LGN; whereas V1 excitatory neurons receive direct input from the LGN but not the basal forebrain.

into consideration with other evidence discussed below, our results indicate a strong direct influence of the basal forebrain on local V1 inhibition.

We previously demonstrated the cell type specificity of AAV-GAD1 and LV-αCamKII on cortical inhibitory and excitatory neurons, and showed that the delivery of YTB through these helper viruses was sufficient to label presynaptic inputs throughout the brain, with an emphasis on intrinsic V1 connectivity (Liu et al., 2013). Here we reconfirmed the cell type specificity of each helper virus and found differenced in the basal forebrain inputs to V1.

The observed projection of basal forebrain to inhibitory, but not to excitatory V1 neurons was not likely due to differences in the two helper viruses used. On the contrary, viral vectors were optimized for their endogenous neurotropism; lentivirus for excitatory neurons and low-titer AAV for inhibitory neurons (Nathanson, Yanagawa, Obata, & Callaway, 2009). Moreover, both helper viruses resulted in retrogradely infected neurons in the LGN; the LGN provided input to both inhibitory and excitatory neurons. Demonstrating that the AAV and lentiviral vectors were both effective at initiating cell type specific retrograde tracing of EnvA-ΔG-RV.

Because previous reports found that only deep V1 injections provided retrograde labeling of basal forebrain neurons (Carey & Rieck, 1987; Rieck & Carey, 1984), we also targeted infragranular layers with our viruses. No discernable difference was found between the distribution of inhibitory and excitatory starter cells in layers 5 and 6.

While no basal forebrain neurons were found to project to excitatory V1 cells, this does not necessarily mean that this connection is not present. Our method of complementation of EnvA-ΔG-RV with the B19 strain of the rabies glycoprotein (B from YTB) is most likely to label stronger connections, based on the number of synaptic inputs (Liu et al., 2013; also see Lyon et al., 2010; Lyon & Rabideau, 2012; Liu, Arreola, Coleman, & Lyon, 2014). Therefore, it is

possible for weaker connections to be missed. In support of this, a slight loss in the average number of basal forebrain and LGN cells labeled by helper virus complementation of EnvA-ΔG-RV, was observed compared to ΔG-RV, which does not require complementation (compare Tables 1.1 and 1.2). In addition, studies using transgenic mice to provide higher levels of the rabies glycoprotein did show a basal forebrain input to three types of V1 excitatory neurons (Kim et al., 2016).

A stronger or exclusive direct synaptic input to infragranular inhibitory neurons as our results suggest, is consistent with other work indicating a greater effect of the cholinergic system on inhibition in V1. While an excitatory effect of acetylcholine has been observed, this is likely most predominant in layer 4 where there is an abundance of nicotinic receptors found on excitatory neurons (Disney et al., 2007). However, in layers 2/3, 5, and 6, M1 and M2 type muscarinic receptors are found predominantly on inhibitory neurons, despite inhibitory neurons only representing ~20% of the V1 neural population (Disney et al., 2006, 2007, 2012). Consistent with this anatomy, in layers 2/3, 5, and 6, acetylcholine largely leads to suppressed V1 cell activity (Disney et al., 2012). Moreover, in layer 5 acetylcholine release was shown to amplify the inhibitory signal and decreases the excitatory and sensory responsiveness of pyramidal neurons (Lucas-Meunier et al., 2009). This inhibitory effect could result from direct synaptic contact onto local deep layer inhibitory neurons, which in turn suppress neighboring excitatory pyramidal cells.

These results show a direct projection from BF neurons to V1 inhibitory neurons, implicating cholinergic modulation of inhibitory interneuron function in visual processing. However, given the reduced number of cells found in the LGN from the excitatory cell-type promoter, further analysis is required to confirm the relative strength of the projection from the

LGN compared with the inhibitory cell-type promoter, as well as confirmation of the virus' ability to transsynaptically label a sufficient number of input neurons for comparison. The method used here was limited due to the helper virus infection rate; as such, we would like to explore a newly developed enhanced methodology to label a greater number of projection neurons from our injection site (Kim et al., 2016).

CHAPTER 2: ENHANCED METHOD FOR CELL-TYPE SPECIFIC TRACING CONFIRMS INHIBITORY NEURONS ARE THE PRIMARY TARGET OF BASAL FOREBRAIN INPUTS TO PRIMARY VISUAL CORTEX

The basal forebrain has been previously shown to project directly onto V1 neurons in a variety of animal models (Henderson, 1981; Tigges et al., 1982; Carey & Rieck, 1987; Dreher, Dehay, & Bullier, 1990) and play a role in attention modulation and plasticity in V1 (Sillito & Kemp, 1983; Bear & Singer, 1986; Roberts et al., 2005; Herrero et al., 2008; Newman et al., 2012; Chubykin et al., 2013; Avery, Dutt, & Krichmar, 2014). The cholinergic characteristic of the basal forebrain suggests this to be the primary nature of the projection (Henderson, 1981; Sarter, Hasselmo, Bruno, & Givens, 2005; Pinto et al., 2013), and indeed cholinergic effects have been shown in vivo to alter response gain (Sato et al., 1987a; Sato et al., 1987b; Roberts et al., 2005; Soma et al., 2013), while optogenetic studies of transgenic mice indicate a role in enhanced visual perception (Pinto et al. 2013; Lin et al., 2015). Our ability to further analyze such a projection is crucial to our understanding of the role of acetylcholine on cortical function and visual cognition (Mesulam et al., 1983b; McGaughy et al., 2000; Jones, 2004; Herrero et al., 2008; Hasselmo et al., 2011).

Previous results from this lab have shown that these basal forebrain projections target V1 inhibitory neurons, but not excitatory V1 neurons (Lean et al., 2015; Lean et al., 2019). These results are consistent with the predominant location of cholinergic receptors (AChR) localized on inhibitory neurons (Disney et al., 2006; Disney et al., 2008; Disney et al., 2012; Disney et al., 2014). The results from the prior study were based on 12 rodent cases utilizing a G-deleted Rabies Virus (Δ G-RV) pseudotyped with EnvA to target rabies infection to specific starter cell

types and trans-synaptically label only the direct presynaptic inputs (Wickersham et al., 2007; Liu et al., 2013; Lean et al., 2019). However, the monosynaptic rabies method used in our prior studies may have labeled only a fraction of presynaptic neurons due to the limitations of the G-protein (Callaway & Luo, 2015; Miyamachi et al, 2013; Watabe-Uchida et al., 2012; Kim et al., 2016). As such, though able to confirm the location and nature of the projection, prior viral methodology may not accurately portray the true strength of the projection with regard to the direct visual cortical targets.

A newly designed ‘optimized’ rabies glycoprotein, oG, was developed to improve the efficiency of long-distance transsynaptic tracing with EnvA pseudotyped rabies virus (Kim et al., 2016). The oG has been shown to increase expression levels of the rabies glycoprotein in starter cells, which resulted in a four- to nine-fold improvement in retrograde labeling of presynaptic inputs (Kim et al., 2016). In this study, we utilized the oG to enhance our labeling of input neurons and re-examine whether V1 excitatory neurons receive any direct synaptic input from the basal forebrain. Although the results confirmed our prior findings regarding the predominantly inhibitory targets of this projection, enhanced labeling allowed for further understanding of the relative strength of direct synaptic labeling to inhibitory and excitatory neurons and provided further insight into the nature of acetylcholine release on both general cortical cell types.

2.1 Materials and Methods:

3 adult rats and 10 adult mice of both sexes were used following procedures approved by the University of California, Irvine Institutional Animal Care and Use Committee and the Institutional Biosafety Committee, and the guidelines of the National Institutes of Health.

2.1a Surgical Procedures

For the three rat cases, anesthesia was induced and maintained with 0.3% isoflurane and 0.7% nitrous oxide throughout the procedure. Once anesthetized, animals were placed in a stereotaxic head-holder and a craniotomy was performed of the neocortex bilaterally under sterile conditions. Temperature was kept at 37˚C throughout the procedure using a heating pad (Harvard Apparatus, Holliston, MA, USA). Glass pipettes with tips broken to approximately 20 µm were filled with virus and inserted through dura using a computer-controlled micro-positioner attached to a KOPF stereotaxic arm. Coordinates between 5.54 and 7.36mm posterior from Bregma and 2.60 and 4.45mm lateral to the midline were used. Injections of either LV- α CamKII-YToG (N=1) or AAV-GAD-YToG (N=2) were made at a depth of approximately 700 and 1200 µm using a computer-controlled micro-positioner attached to a KOPF stereotaxic arm and a volume of approximately 0.8-1.2µl was administered via a pressure injecting pico-pump. Similarly, for the ten mouse cases, anesthesia was induced and maintained with 0.3% isoflurane throughout the procedure. Once anesthetized, animals were placed in a smaller stereotaxic head-holder and a craniotomy was performed bilaterally of the neocortex under sterile conditions. Coordinates between 3.0 and 4.5mm posterior from Bregma and 1.25-3.25mm lateral to the midline were used. Injections of either LV- α CamKII-YToG (N=2), LV- α CamKII-YTB (N=5), or AAV-GAD-YTB (N=4) were made at a depth of approximately 500 and 700 µm using a computer-controlled micro-positioner attached to a KOPF stereotaxic arm and a volume of approximately 0.8-1.2µl was administered via a pressure injecting pico-pump.

For all cases, dental cement was used to seal the craniotomy following the initial helper virus injection and the animals were revived for a 21-day recovery period to allow the virus to spread before the injection of the rabies virus. Each animal was anesthetized as before, and under

sterile conditions the acrylic skull cap removed and EnvA injections of ~0.5µl made as close as possible to the original helper virus injected location based on the coordinates and landmarks described above. The craniotomy was then covered with fresh Tecoflex, resealed with dental acrylic, and the animals revived. A final survival period ranging from 7 to 10 days followed.

2.1b Viruses

For the 10 cases shown with the YTB helper viruses, GAD1-YTB (7382 bp) and αCamKII-YTB (7500 bp) were sub cloned into adeno-associated virus (AAV) and lentiviral (LV) backbones to make AAV-GAD1-YTB (11026 bp) and LV-αCamKII-YTB (12.3kb), as described previously (Liu et al., 2013). From these plasmids, serotype 9 AAV and VSV-G pseudotyped LV particles were prepared and purified by the Gene Transfer Targeting and Therapeutics Core at the Salk Institute of Biological Studies (La Jolla, CA) yielding a titer of $9x10^9$ genome copies/mL for AAV and $2x10^{10}$ transducing units/ml for LV.

The 5 YToG cases shown utilized a similar virus, but with an optimized glycoprotein to allow for greater efficiency of transsynaptic spread by more than an order of magnitude compared to the original virus (Kim et al., 2016). To generate AAV-GAD-YToG and LV-αCamKII-YToG we used ythe following procedures:

Subcloning procedure for AAV-GAD1- YToG

First we excised a HindIII fragment (5173 bp) from AAV-GAD1-YTB (11026 bp), resulting intermediate plasmid rAAV-(B) (5853 bp) for later insertion of oG. The HindIII cuts into the 5'region of the rabies virus B glycoprotein cDNA, but this part of the cDNA will be reintroduced in the last cloning step (below).

Second, we used PCR to form the major part of oG cDNA (1491 bp) from TVAmCherry-2a-oG (obtained via Addgene curtesy of Ed Callaway) to contain restriction sites for HindIII (5') and BsiWI (3').

Forward primer: 5'-CCGAAAGCTtGGCCCCTGGAGTCC-3' (HindIII site in red; lower case t from B cDNA → silent mutation)

Reverse primer: 5'-ctcgtacgTTAGAGCCGTGTCTCGCCCCC-3' (BsiWI site in red; capital letters show 3'end of the oG cDNA)

Third, we cut both rAAV-(B) plasmid and the PCR product with HindIII (in NEB buffer 2.1) and BsiWI (in NEB buffer 3.1) and inserted the oG cDNA into the plasmid to obtain rAAV-oG (5775 bp).

Fourth, rAAV-oG was cut with HindIII, dephosphorylated (to avoid self-religation of the plasmid), and the HindIII fragment from above (step 1) was inserted to obtain rAAV-GAD1-YToG (10948 bp).

Subcloning procedure for LV-αCamKII-***YToG***

First, our stock plasmid, LV- αCamKII-YTB, was cut with BamHI (5' overhang) and AscI (5' overhang, compatible with BssHII).

Second, YToG was excised from pAAV-GAD1-YToG (above) with BamHI (5') and BssHII (3').

Third, the BamHI/BssHII fragment was for YToG (3299 bp) was ligated into the BamHI/AscI backbone plasmid of LV- αCamKII-YTB (9420 bp) to yield LV- αCamKII-YToG BamHI AscI-BssHII (12719 bp).

Fourth, this plasmid was then transformed into Stbl2 cells via electroporation at 30° C and Stbl3 cells by heat-shock (37° C).

Fifth, an excision of the unwanted 3'-ITR from AAV to obtain LV- αCamKII-YToG BGH (12607 bp

Sixth, the bovine growth hormone (BGH) poly-A sequence was then removed to obtain LV- αCamKII-YToG (12182 bp).

2.1c Histology and antibody reporting

For histology, animals were deeply anesthetized with Euthasol (390 mg/ml of sodium pentobarbital and 50 mg/ml of sodium phenytoin, ip; Vedco Inc., Saint Joseph, MO, USA) and perfused transcardially, first with saline, then followed by 4% paraformaldehyde in phosphate buffer (PB; pH 7.4). Brains were removed and cryoprotected in 30% sucrose for ~48hr prior to sectioning.

Brains were cut coronally at 40µm thickness and saved in four series separated by 120µm. A series of every fourth section was processed for DAPI and an additional series processed for PV using the anti-PV rabbit polyclonal antibody (1:1000; Swant). Immunopositive neurons were revealed using fluorescent secondary Alexa Fluor 350 goat anti-rabbit IgG (1:500; Invitrogen). To enhance visualization of yellow fluorescent protein (YFP) the same sections were also processed for the anti-GFP chicken polyclonal antibody (1:1000, Novus Cat#NB100-1614, RRID:AB523902; tested on transgenic mice expressing recombinant GFP: Immunogen affinity purified) and revealed using Alexa Fluor 488 goat anti-chicken IgG (1:500; Invitrogen). The mCherry reporter from rabies virus was not enhanced through immunofluorescence. Rabies

virus infected neurons could be visualized in all sections without processing. Sections were cover-slipped in PVA-DABCO (Sigma-Aldrich) to preserve fluorescence.

2.1d Data Analysis

Sections were examined using fluorescent microscopy (Zeiss Axioplan, Oberkochen, Germany) with 10x (0.45NA) and 20x (0.8NA) objectives and cell positions reconstructed using Neurolucida software (MicroBrightField, Willston, VT) offline. To limit bleaching of fluorescence, images of whole sections were captured with high-power black and white digital camera (Cooke SensiCam QE) and stitched together through the Virtual Slide module.

Confirmation of V1 injection sites and the locations of the LGN and basal forebrain were based on the atlas by Paxinos and Franklin (2001).

2.2 Results

Using the optimized virus, we confirmed that a large number of neurons in the basal forebrain project directly to V1 inhibitory neurons, but few to none project directly to excitatory neurons (Tables 2.1 and 2.2). Additionally, we found significantly enhanced labeling of LGN inputs to both inhibitory and excitatory neurons compared with our previous virus ($p<0.05$), which allows us to compare the strength of the projection from the basal forebrain between the two oG viruses. In our prior results, there was a comparable amount of LGN labeling using both excitatory and inhibitory promotor viruses (Lean et al., 2019). With the enhancement of oG, there was a shift in the relative strength of the projection from the basal forebrain and LGN so that it is no longer equal in strength, but rather corresponds with our previous understanding that

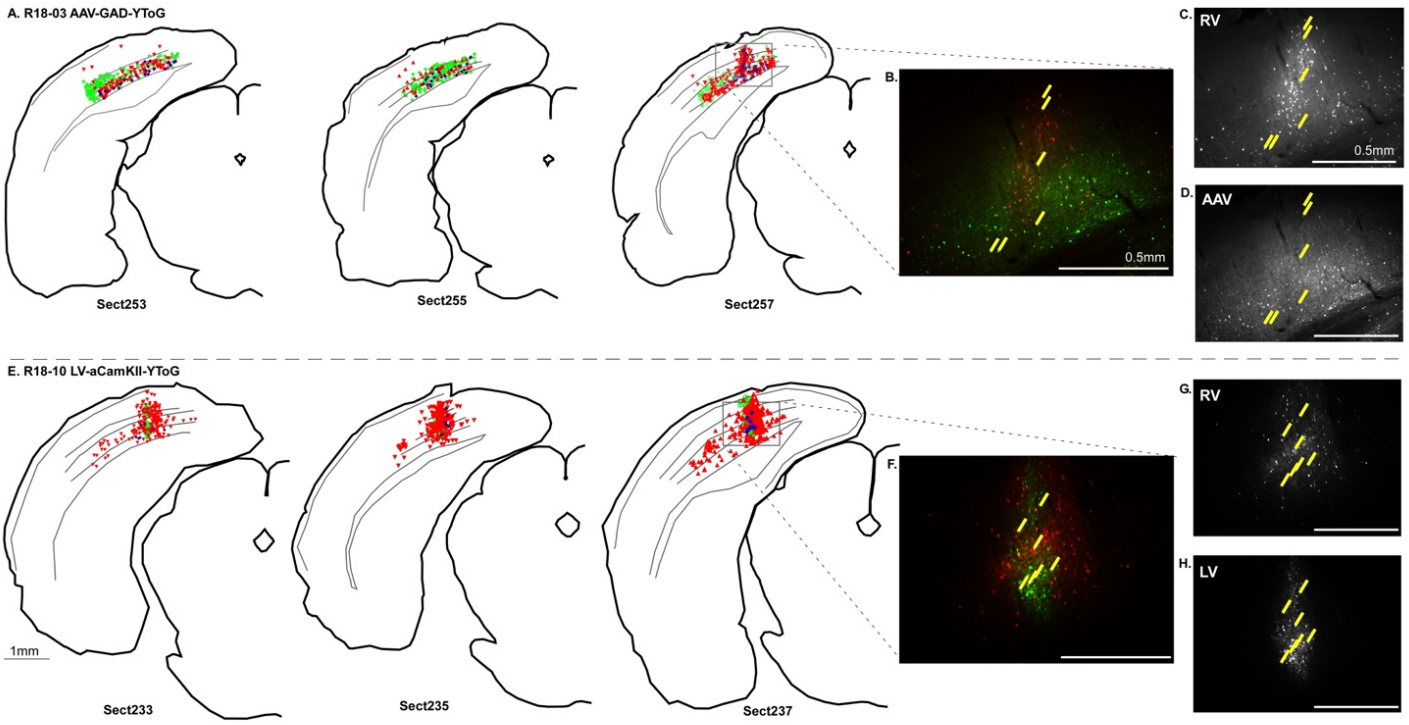

Figure 2.1 A Reconstruction of the injection site locations in V1 with AAV-GAD-YToG infection (A) and LV-aCamKII-YToG infection (E). Rabies virus (C,G) and specific helper viruses (D,H) labeling are included to illustrate the overlap in labeling (C,F) and indicate that the injection sites extended through layers 4-6. Yellow markers are included to indicate a few of the double-labeled (starter cells) in each case.

the LGN provides the main cortical input to V1 (Xu et al., 2001; Casagrande et al., 2005; Nassi et al., 2006; Marshel et al., 2012).

2.2a oG Enhanced Labeling of Projection Neurons to Both Excitatory and Inhibitory V1 Cells

The number of projection neurons from LGN to V1 identified using the optimized glycoprotein was significantly greater than the previous version of the virus (Tables 2.1 and 2.2; $p<0.05$). This increase indicates the is used as a control for proper injection location, as the LGN provides a known projection to V1 layers 4 and 6 (Nassi et al., 2006; Callaway, 2005; Wiesel, T.N. & Hubel, D.H., 1966; Van Essen et al., 1992). Given the presence of a significant number of retrogradely labeled cells in V1, we can confirm that our injection reached deep layers in V1.

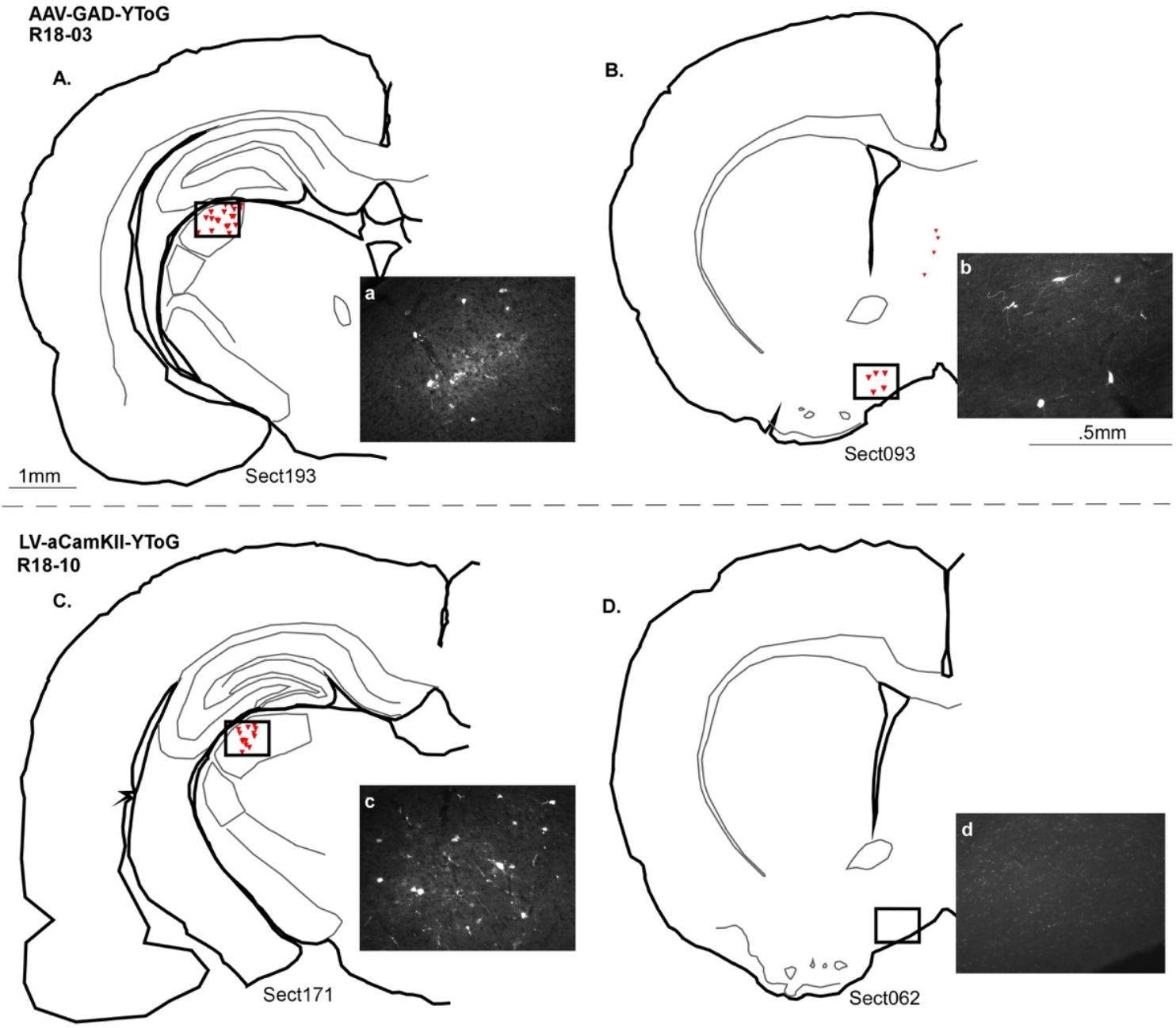

Figure 2.2: Reconstruction of retrogradely-infected neurons in the LGN (A,C) and basal forebrain (B,D). Digital images of rabies virus infected neurons in the LGN (a,c) and BF (c,d) from regions outlined with rectangles in the schematic diagrams are included. Note that in the case injected with LV-aCamKII-YToG, there is no visible labeling in the basal forebrain.

Additionally, the number of starter cells labeled with the oG was significantly greater than with the prior virus ($p<0.03$). Specifically, the number of starter cells in L6 is significantly increased ($p<0.03$). This is important because L6 neurons receive a known projection from the LGN (Nassi et al., 2006; Callaway, 2005; Wiesel, T.N. & Hubel, D.H., 1966; Van Essen et al.,

1992), so enhancement of starter cell counts in this region account for the significant increase in retrograde labeling to LGN neurons.

2.2b AAV-GAD-YToG

The optimization of the GABAergic helper virus enhanced the long-range labeling of LGN and BF projection neurons to inhibitory cells in V1 (Table 2.1A). An average of 56 retrograde infected neurons were found in the basal forebrain using the oG, compared with 24.2

Table 2.1: Number of retrogradely infected neurons in the BF and LGN projecting to V1 starter cells in layers 4, 5, and 6. (A) 2 cases using the oG with the GAD promoter. (B) 5 cases using the YTB helper virus strain with the GAD promoter for comparison. (C) 3 cases using the oG with the aCamKII promoter. (D) 5 cases using the YTB helper virus strain with the aCamKII promoter for comparison.

A.	AAV-GAD-YToG	BF	LGN	Starter Cells	L4	L5	L6
	R18-03L	58	102	235	15	119	110
	R18-03R	54	114	306	28	105	155
B.	AAV-GAD-YTB	BF	LGN	Starter Cells	L4	L5	L6
	R16-28L	75	31	180	4	83	93
	M11-20	23	22	30	3	14	13
	M12-05	6	2	63	7	22	34
	M12-06	13	7	60	4	17	39
	M12-17	4	32	77	9	44	24
C.	LV-aCamKII-TYoG	BF	LGN	Starter Cells	L4	L5	L6
	R18-10L	0	168	80	19	31	20
	M18-01L	2	12	115	4	8	103
	M18-01R	1	36	114	24	22	44
D.	LV-aCamKII-YTB	BF	LGN	Starter Cells	L4	L5	L6
	M11-19	0	4	44	6	16	22
	M12-09	0	8	89	3	48	38
	M12-15	0	12	145	32	53	60
	M12-16	0	4	42	13	16	13
	M12-26	0	4	23	8	11	4

using the YTB version of the virus (Table 2.2). Additionally, the number of retrograde infected cells in the LGN increased nearly 10-fold using the oG virus, to an average of 108 compared with 18.8.

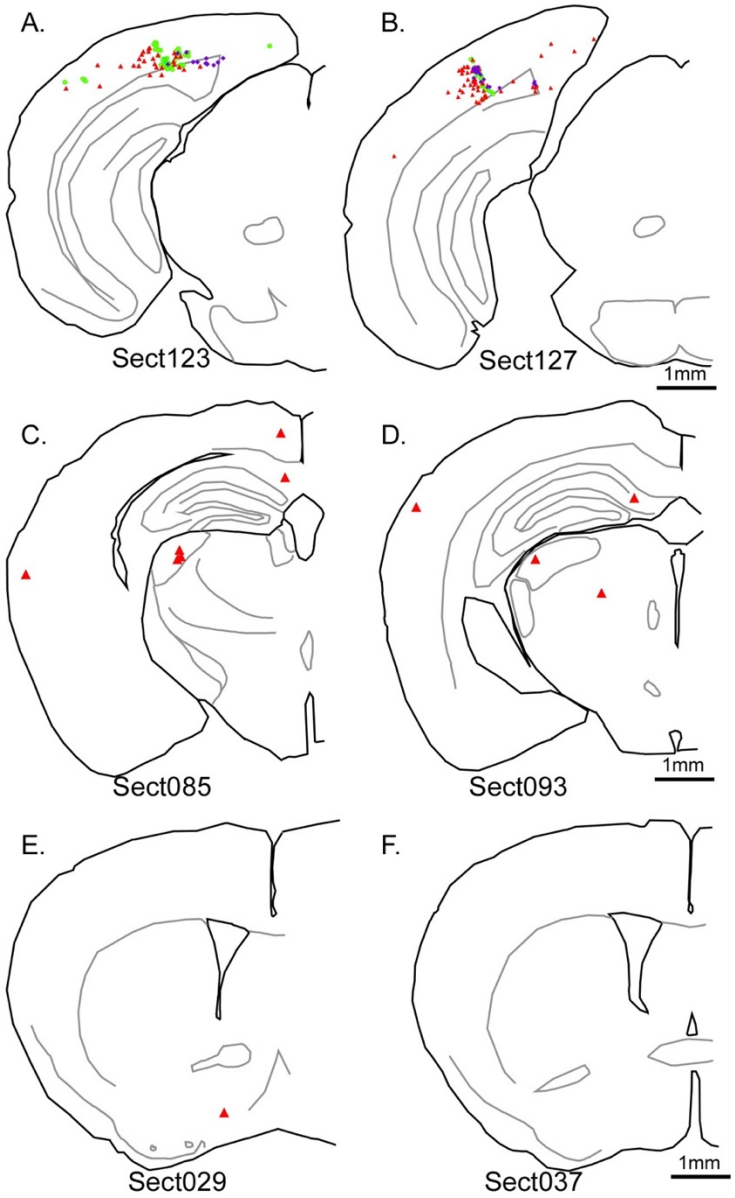

Figure 2.3 Series of sections labeled with LV-aCamKII-YToG injections in mouse V1. (A,B) 2 sections showing the injection site of LV-aCamKII-YToG (green circles), EnvA-△G-mCherry (red triangles) and double-labeled starter cells (purple diamonds). (C,D) 2 sections showing retrograde-labeled cells in LGN. (E,F) 2 sections showing BF area following LV-aCamKII injection V1. Note that the cell labeled in section 029 (E) is the only BF neuron found with retrograde labeling in this case (See section 037 for comparison). All sections are from #M18-01R.

Figure 2.1A provides an example of a case labeled with the new GAD promoter helper virus and the subsequent injection of EnvA Rabies virus. Note that starter cells are visible across multiple layers of V1, including layers 4, 5 and 6 (Figure 2.1B-D). When compared with previous cases, the number of starter cells labeled is substantially greater across all cases (Table 2.1A). This led to increased labeling of long-range projection neurons including the BF and LGN shown in Figures 2.2A and 2.2B.

2.2c LV- α CamKII-YToG

The optimization of labeling to V1 neurons using the excitatory promoter showed enhanced LGN labeling and an increase in BF labeling compared with the original YTB virus. An average of 1 retrograde infected neuron was found in the basal forebrain across three different cases, which is a notable increase from zero found using the YTB helper virus strain (Table 2.1C,D). Additionally, the average number of retrogradely infected neurons in LGN increased 10-fold, with a greater increase than that seen with the AAV-GAD-YToG strain (Table 2.2).

Figure 2.1E provides an example of a case labeled with the α CamKII promoter helper virus and the subsequent injection of EnvA Rabies virus. A similar number of starter cells was found in this case compared with the exemplar shown in Figure 2.1A with the GAD helper virus, including a well-distributed proportion of starter cells across all cortical layers. Additionally, this case has a substantial amount of labeling in the LGN and across V1 (Figure 2.2C). However, this example case did not have a single labeled cell in the basal forebrain (Figure 2.2D).

Figure 2.3 provides an additional example of retrograde labeling from α CamKII promoter helper virus injection and subsequent injection of EnvA Rabies virus into V1. This figure provides the tracing of two sections from the V1 injection site (Figure 2.3A), LGN (Figure 2.3B), and BF (Figure 2.3C), all approximately 300μm apart from one another. This figure is included to demonstrate an example of a case with a single presynaptically-labeled neuron in the BF compared with the previous figure with no BF labeling whatsoever.

2.3 Discussion

The goal of this experiment was to determine the extent of the cell-type specificity of cortical neurons in V1 receiving a direct input from the basal forebrain using enhanced methodology. Previous viral methods allowed us to examine the relationship between the basal forebrain and it's V1 terminals, and demonstrated the virus' ability to label specific projection neurons through presynaptic connections with target neurons (Lean et al., 2019; Liu et al., 2013); however, with limited expression of the G-protein, the strength of the projection was difficult to discern. With the use of the optimized glycoprotein, we reconfirmed direct synaptic input to V1 inhibitory neurons from BF neurons and identified a minimal yet notable projection to V1 excitatory neurons. Via newly devised viral techniques, we are able to examine this relationship

Table 2.2: Average number of cell counts for each region.

Virus Type	BF	LGN	Starter Cells	L4	L5	L6
AAV-GAD-YToG	56	108	270.5	21.5	112	132.5
AAV-GAD-YTB	24.2	18.8	82	5.4	36	40.6
LV-aCamKII-TYoG	1	82	103	15.6	20.3	55.7
LV-aCamKII-YTB	0	6.4	68.8	12.4	28.8	27.4

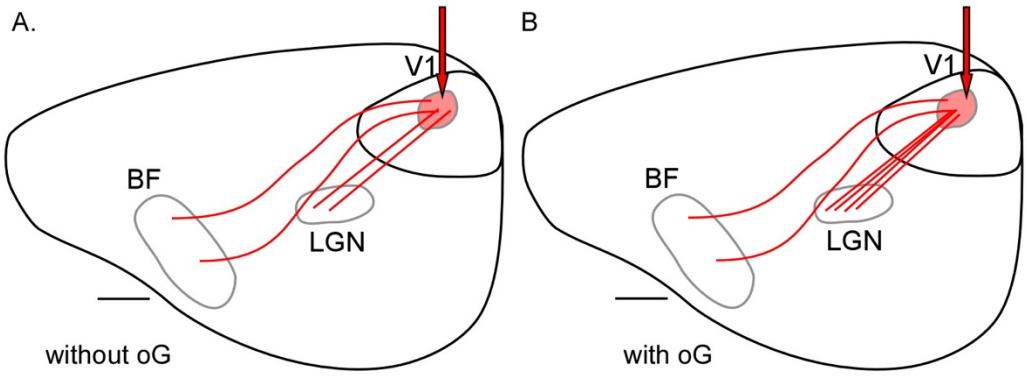

Figure 2.4 Schematic representation of the relative strength of labeling from presynaptic neurons to V1 injection site. (A) In the original strain of the virus, we have a comparable strength of labeling from the LGN and BF neurons types. (B) Using the oG virus, there is an enhanced number of projections neurons from the LGN relative to the number of projection neurons from the BF.

more effectively and determine with greater confidence the relative strength of this projection to inhibitory neurons and the relative weakness of this projection to excitatory neurons.

The overall labeling pattern in the LGN with the two oG viruses (AAV-GAD-YToG and LV- α CamKII-YToG) is very similar (Figure 2A,C), indicating successful retrograde infection of both virus types and allowing us to compare between the two. In our previous results, we noted a similarity in the strength of the projection from the LGN and the BF to inhibitory V1 neurons (Table 2.1B; Figure 2.4A; Lean et al., 2019). However, with improved expression, we note that the relationship between the number of retrogradely labeled cells in the BF and LGN is now significantly different ($p<0.03$) and no longer of comparable strength (Figure 2.4B). Clearly, the enhanced labeling technique confirms the ability to obtain improved infection and transsynaptic spread of the virus (Kim et al., 2016).

Additionally, our results indicate enhanced labeling in starter cells compared with the previous virus used. This is likely a result of the following two features: first, the increased ability for infection via the optogene allows for greater presynaptic labeling; second, the oG virus has no observable toxic effects (Kim et al., 2016) so the starter cell population is healthier following injection than the previous virus. The significant increase in starter cell infection

($p<0.03$), particularly in cortical layer 6, most likely contributed to the increase in retrograde labeling to LGN described earlier, as V1 layer 6 receives a direct projection from the LGN (Thomson, 2010; Xu et al., 2001; Casagrande et al., 2005; Nassi et al., 2006; Marshel et al., 2012).

It is important to note that although the proportion of labeled cells has changed relative to each subregion, the overall amount of labeling is still substantially increased for both regions. This is important to consider as we begin examining the functional role of the BF projection using the same methodology. Perhaps with optimized glycoprotein use in conjunction with optogenetic targeting, the effects on V1 cells during visual perception tasks will be enhanced.

Given the presence of a few excitatory cells receiving BF input, we cannot rule out the potential for a modulatory role of the BF on V1 excitatory neurons as well, particularly in layer 4 thalamocortical pathways (Disney et al., 2007). Our results is consistent with evidence to suggest that these cells provide cholinergic input to V1(Herrero et al., 2008; Thiele, 2009, Newman et al., 2012; Deco & Thiele, 2009; Avery et al., 2014; Soma et al., 2013; Thiele, 2009). It is known that the volume transmission release of acetylcholine is typically not specific to synaptic specialization and reaches both cell types (Disney et al., 2007; Aoki and Kabak, 1992; Beaulieu and Somogyi, 1991; Turrini et al., 2001), and as such there is minimal, yet still present, retrograde labeling due to excitatory cell infection. Alternatively, it is possible that the few BF neurons labeled via excitatory cell-type specific tracing are part of the nicotinic pathway originating in cortical layer 4 neurons (Disney et al., 2006; Disney et al., 2007; Soma et al., 2013; Thiele, 2009). The minimal number of cells found across three separate cases suggest that this is less likely. Instead, it is likely that the direct synaptic connections are limited to inhibitory interneuron subtypes due to the chemoarchitectural analysis of acetylcholine receptors and their

predominant location on inhibitory cell types (Disney et al., 2012; Disney et al., 2006). Taken together, these experiments provide direct evidence for cholinergic modulation in V1. This is consistent with evidence shown that attentional effects mediated by cholinergic projections strongly influence neuronal processing in cortical areas (Herrero et al., 2008; Thiele, 2009, Newman et al., 2012; Deco & Thiele, 2009; Avery et al., 2014; Disney et al., 2012).

CHAPTER 3: SIZE TUNING EFFECTS WITH OPTOGENETIC MANIPULATIONS OF BASAL FOREBRAIN PROJECTION NEURONS TO V1 RECIPIENTS IN RODENT

The primary visual cortex is responsible for orientation selectivity, contrast sensitivity, and size tuning (Sceniak et al., 1999; Chen et al., 2005; Hashemi-Nezhad and Lyon, 2012; Liu et al., 2015) and is thought to play a critical role in early object perception processed in higher visual areas (Series et al., 2003). A variety of interneurons are intrinsically connected via long-range intracortical projections to mediate interactions across visual space and provide contextual modulation of the receptive field (Das and Gilbert, 1999; Series et al., 2003, Lyon et al., 1998) in order to process a wider range of component images. Suppression is used in V1 when a stimulus exceeds the optimal size (Liu et al., 2011; Jones et al., 2001; Sengpiel et al., 1997; Walker et al., 2000). Therefore, a greater understanding of the mechanisms involved in V1 inhibition can illuminate the observed patterns in visual processing and provide insight into how the structural connections lead to functional changes.

One of these potential mechanisms of modulatory effects on inhibitory V1 neurons is the direct projection from the basal forebrain (BF) onto inhibitory neurons in V1 (Lean et al., 2019; Henderson, 1981; Tigges et al., 1982; Carey & Rieck, 1987; Dreher, Dehay, & Bullier, 1990; Do et al., 2016). Iontophoretic release of acetylcholine in primary visual cortex (V1) specifically has been implicated in the direct role of spatial integration (Roberts et al., 2005) and contrast response gain (Soma et al., 2013; Disney et al., 2012; Bhattacharyya et al., 2013). In a study conducted by Roberts et al. (2005), externally applied acetylcholine in marmoset V1 caused neurons to respond better to visually displayed bars of shorter length. This led to the conclusion that acetylcholine plays a role in controlling spatial integration and is likely due to activation of

cortical inhibitory neurons (Disney et al., 2006; Disney & Aoki, 2008; Silver et al., 2008; Newman et al., 2012).

Additional studies of acetylcholine application in vivo have illustrated a strong effect on response gain (Soma et al., 2013; Pinto et al., 2013; Disney et al., 2012; Martinez-Trujillo & Treue, 2002). Acetylcholine release decreased the visual response of individual cells and modulated the gain of the contrast-response function, which led to the conclusion that acetylcholine acts as a gain controller in rodent (Soma et al., 2013; Disney et al., 2012).

Cholinergic projection neurons have also been shown to enhance visual perception. Pinto et al. (2013) showed that specific activation of cholinergic neurons in the basal forebrain was sufficient to enhance cortical processing and visual discrimination in awake animals. Additionally, their results strongly suggest that the basal forebrain activation-induced perceptual improvement is mediated partly by the cholinergic projection to V1 (Pinto et al., 2013). These results, combined with those from prior studies, provide a better understanding of the overall effects of acetylcholine release in V1 and its' role in visual processing. However, the role of laminar distinctions remains unclear. Additionally, the effect of cholinergic activation on aperture tuning, a known feature of V1 processing, has not been addressed.

Each cortical layer has a different proportion of acetylcholinergic receptors (AChRs) (Disney et al., 2006) which in turn lead to a different functional response (Disney et al., 2007; Disney & Reynolds, 2014). The exact role of acetylcholinergic release across multiple visual cortical layers is expected to change based on the density of these distinct acetylcholine receptors (Disney et al. 2014; Disney et al., 2007; Disney et al., 2006). Despite diffuse volume transmission (Descarries et al., 1997; Sarter et al., 2009), cholinergic projections have some degree of anatomical specificity based on the location of the two types of acetylcholine receptors

(Disney et al., 2008; Bhattacharyya et al., 2013). As a result, the effects of cholinergic release in different V1 layers may cause varying changes in a cell's preferred stimulus type.

This study utilizes a G-deleted rabies virus construct to retrogradely label projection neurons from their terminals in V1 (Liu et al, 2013; Wickersham et al., 2007). The rabies virus is tagged with a light-sensitive channel rhodopsin in order to selectively activate only those neurons that originate in the basal forebrain (Osakada et al., 2011). The goal of this study was to determine whether basal forebrain activation and it's known cholinergic release would change the preferred stimulus size. Our results indicate that there is a change in preferred stimulus size.

3.1 Materials and Methods:

4 adult rats of both sexes were used following procedures approved by the University of California, Irvine Institutional Animal Care and Use Committee and the Institutional Biosafety Committee, and the guidelines of the National Institutes of Health were followed. All rats were housed individually in a plexiglass cage and maintained in a 12-hour light/dark cycle (lights on from 06:30 to 18:30h) at an ambient temperature of 21.5+/-0.8˚C and a relative humidity of 50%.

3.1a Surgical Procedures

Anesthesia was induced and maintained with 0.3% isoflurane and 0.7% nitrous oxide throughout the procedure. Temperature was kept at 37˚C throughout the procedure using a heating pad (Harvard Apparatus, Holliston, MA, USA). Once anesthetized, animals were placed in a stereotaxic head-holder and a craniotomy was performed over the right caudal half of the neocortex under sterile conditions. Glass pipettes with tips broken to approximately 20 μm were filled with virus and inserted through dura using a computer-controlled micro-positioner attached

to a KOPF stereotaxic arm. Coordinates between 5.54 and 7.36mm posterior from Bregma and 2.60 and 4.45mm lateral to the midline were used to target V1 (Figure 3.2A). G-deleted ChR injections were made at a depth of approximately 700 and 1200 µm using a computer-controlled micro-positioner attached to a KOPF stereotaxic arm and a volume of approximately 0.8-1.2µl was administered via a pressure injecting pico-pump in the right hemisphere. All 4 rats were given 4 injections of G-deleted EnvA with ChR, which allowed for selective retrograde infection of the opsin to projection neurons. After injection, dental cement was used to seal the craniotomy and the animals were revived for a 7-day recovery period to allow the virus to spread.

Prior to electrophysiological recordings, a small, custom-made plastic 3D-printed chamber was glued to the exposed skull via dental cement in order to keep the animal from moving during recordings. Similar anesthetic procedures were utilized during this chamber application surgery and animals were allowed ~24 hour recovery prior to recordings.

3.1b Viruses

G-deleted Rabies virus was used to retrogradely label input neurons to the injection site via previously described methods (Liu et al, 2013). Viruses were grown in the lab from existing stock and concentrated to a titer range of ~5 x 10^9 infectious units/ml following published protocols (Osakada et al., 2011; Wickersham et al., 2010). The virus has been modified so that the G-protein is deleted and replaced with a gene for the fluorescent protein mCherry as well as the optogene Channelrhodopsin (Figure 3.1).

Figure 3.1: Diagram of G-deleted rabies virus.

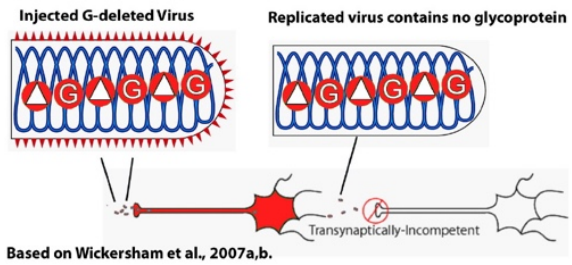

3.1c Electrophysiological recording

Rats were initially anesthetized via similar methods described above and placed into a custom-made hammock and secured in a stereotaxic apparatus using the secured chamber. A single tungsten electrode was inserted into a small craniotomy above the visual cortex where the previous viral injections were made. A second craniotomy was made at approximately the level of Bregma and 1.0mm lateral on the ipsilateral side as the injection of ChR. An optic fiber was inserted at an approximate depth of 8mm below cortical surface in order to reach the basal forebrain and selectively activate presynaptically-labeled neurons (Figure 3.2B). Once the electrode and optic fiber were both inserted, the chamber was filled with sterile saline and the animal was kept under light sedation (0.05% isoflurane and 0.7% nitrous oxide). EEK and EKG were monitored throughout the experiment.

Data was acquired using a 32-Channel Scout Recording System (ThorLabs, NJ, USA). The spike signal was band-pass filtered from 500 Hz to 7 kHz and stored on a computer hard drive at 30 kHz sampling frequency. Spikes were sorted online in Trellis (Ripple, UT, USA) while performing visual stimulation. Visual stimuli were generated in Matlab (Mathworks, USA) using Psychophysics Toolbox (Brainard, 1997; Pelli, 1997; Kleiner et al., 2007) and displayed on a gamma-corrected LCD monitor (55 inches, 60 Hz) at resolution 1920 x 1080 pixels and 52 cd/m^2 mean luminance. Stimulus onset times were corrected for LCD monitor delay using a photoresistor and microcontroller (in-house design).

For recordings of visually evoked responses, cells were first tested for visual responsiveness with 100 repetitions of a 500ms bright flash stimulus (105 cd/m^2). Receptive fields for visually responsive cells were located using square-wave drifting gratings, after which optimal orientation/direction, spatial, and temporal frequencies were determined using sine wave

gratings (Figure 3.2E for orientation, 3.2F for aperture, spatial and temporal frequency tuning not shown). Optimal orientation and direction selectivity were determined using 8 trials of stimulus presentations at 22.5˚ increments presented for 500ms with a 1s interval in between each stimulus. Spatial frequencies tested were from 0.001-0.5 cycles/˚ with the same intervals of presentation and rest described above. Temporal frequencies tested were 0.1 to 10 cycles/s with the same intervals of presentation and rest described above. With these optimal parameters, size tuning was assessed using sizes of 1-110˚ and 100% contrast. With the optimal size, temporal, and spatial frequencies, and at high contrast, the orientation selectivity of the cell was tested again to ensure optimal parameters.

3.1d Optogenetic Activation via Channelrhodopsin

After determining optimal stimulus parameters for the target cell being recorded, a series of trials was completed to determine the optimal stimulus orientation (using 8 trials of stimulus presentations at 22.5˚ increments presented for 500ms with a 1s interval in between each stimulus) with no laser activation, followed by 120 seconds of rest. Then, the same trial was run with 5mW laser stimulation accompanying each stimulus presentation, followed by a 120 second rest period. This was repeated for the 10mW and 15mW laser conditions as well. The same pattern was followed with aperture tuning.

In cases with multiple days of recordings, animals were allowed to recover overnight before continuing records on the next day. Electrode and optic fiber placement were approximately the same on the next day; however, given the potential for tissue shift under the skull, the exact coordinates were not recorded and cortical appearance was used as the primary guide for electrode and fiber placement.

3.1e Histology and antibody reporting

For histology, animals were deeply anesthetized with Euthasol (390 mg/ml of sodium pentobarbital and 50 mg/ml of sodium phenytoin, ip; Vedco Inc., Saint Joseph, MO, USA) and perfused transcardially, first with saline, then followed by 4% paraformaldehyde in phosphate buffer (PB; pH 7.4). Brains were removed and cryoprotected in 30% sucrose for ~48hr prior to

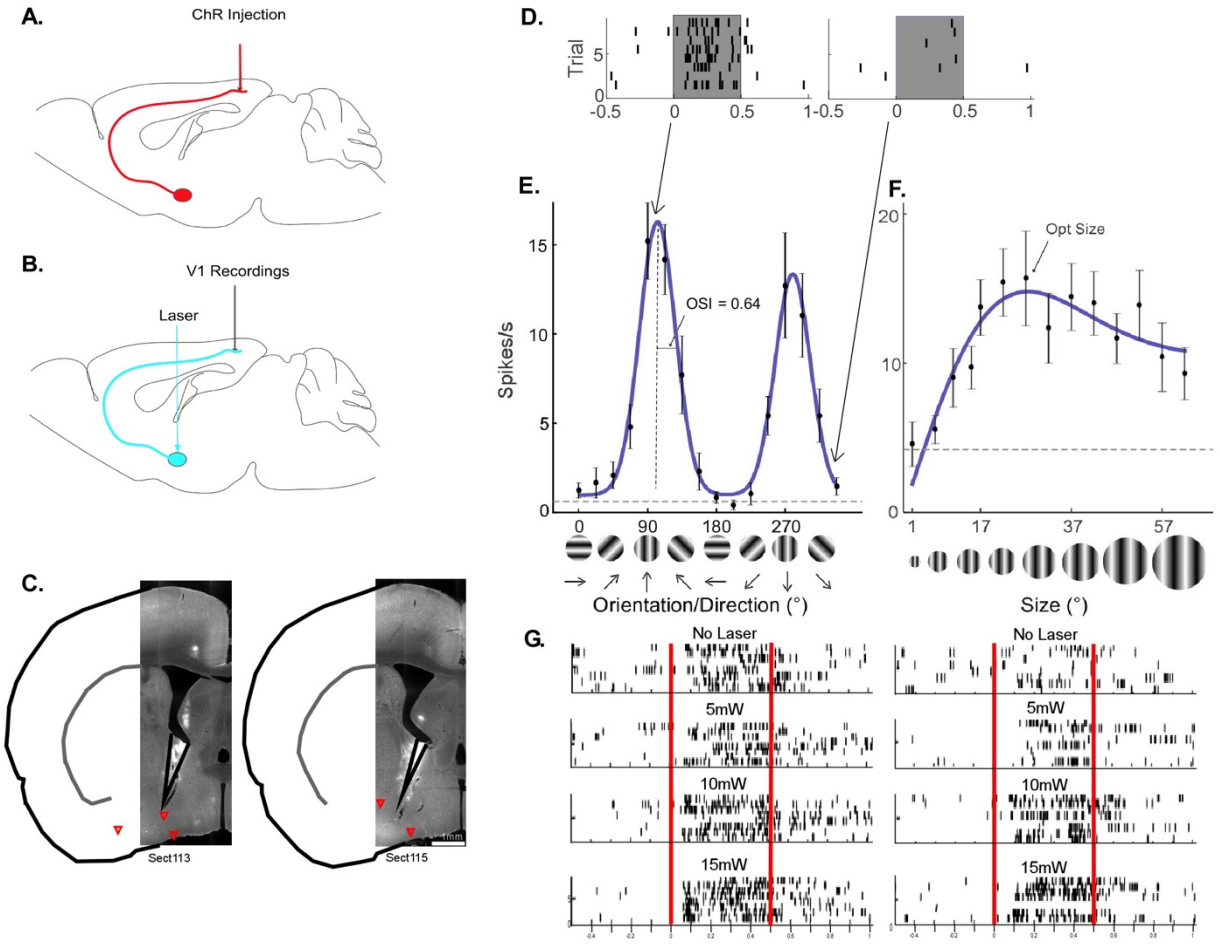

Figure 3.2: Depiction of methods for optogenetic activation and recording experiments. (A) G-deleted RV with Channelrhodopsin was inserted into V1 to allow for infection of presynaptically connected BF neurons. Then, 7-10 days after initial infection, the scull was reopened and an electrode was inserted into the injection site, along with a laser fiber to target the labeled BF neurons. (C) Fluorescent images of an examplar case, in which the fiber tract is visible to the BF. Note the presence of cells labeled with the G-deleted RV with ChR in the BF adjacent to the laser stimulation site. (D-F) Example of optimal stimulus parameter determination for a cell in V1. For each trial, the stimulus presentation is represented by the grey bars (D) and the corresponding stimulus parameter is shown in the bottom of (E) and (F). Increased firing rate at the cell's preferred parameters are recorded and a tuning curve is created (E for orientation tuning, F for Aperture tuning). (G) When combined with laser activation, the amount of firing is recorded when the stimulus and the laser are presented simultaneously, delineated by the red bars. Data from 2 cells is included here.

sectioning.

Brains were cut coronally at 40µm thickness and saved in four series separated by 120µm. A series of every fourth section was processed for DAPI and an additional series processed for PV using the anti-PV rabbit polyclonal antibody (1:1000; Swant). Immunopositive neurons were revealed using fluorescent secondary Alexa Fluor 350 goat anti-rabbit IgG (1:500; Invitrogen). Confirmation of the cholinergic cell type in labeled basal forebrain neurons was obtained in one exemplar case using an anti-Choline Acetyltransferase (ChAT) rabbit polyclonal antibody (1:250; Millipore) and immunopositive neurons were revealed using fluorescent secondary Alexa Fluor 594 anti-rabbit IgG (1:1000; Invitrogen). To enhance visualization of yellow fluorescent protein (YFP) the same sections were also processed for the anti-GFP chicken polyclonal antibody (1:1000, Novus Cat#NB100-1614, RRID:AB523902; tested on transgenic mice expressing recombinant GFP: Immunogen affinity purified) and revealed using Alexa Fluor 488 goat anti-chicken IgG (1:500; Invitrogen). The mCherry reporter from rabies virus was not enhanced through immunofluorescence. Rabies virus infected neurons could be visualized in all sections without processing. Sections were cover-slipped in PVA-DABCO (Sigma-Aldrich) to preserve fluorescence.

3.1f Data Analysis

Sections were examined using fluorescent microscopy (Zeiss Axioplan, Oberkochen, Germany) with 10x (0.45NA) and 20x (0.8NA) objectives and cell positions reconstructed using Neurolucida software (MicroBrightField, Willston, VT) offline. To limit bleaching of fluorescence, images of whole sections were captured with high-power black and white digital camera (Cooke SensiCam QE) and stitched together through the Virtual Slide module.

Figure 3.3: Digital images of choline acetyltransferase in basal forebrain. (A) Overview of the section containing the basal forebrain. (B) Retrograde labeling of BF neurons from V1 injection of G-RV. (C) ChAT labeling in BF via antibody staining (Rb anti ChAT 1:250 concentration). (D) Overlay of the RV and ChAT labeled cells.

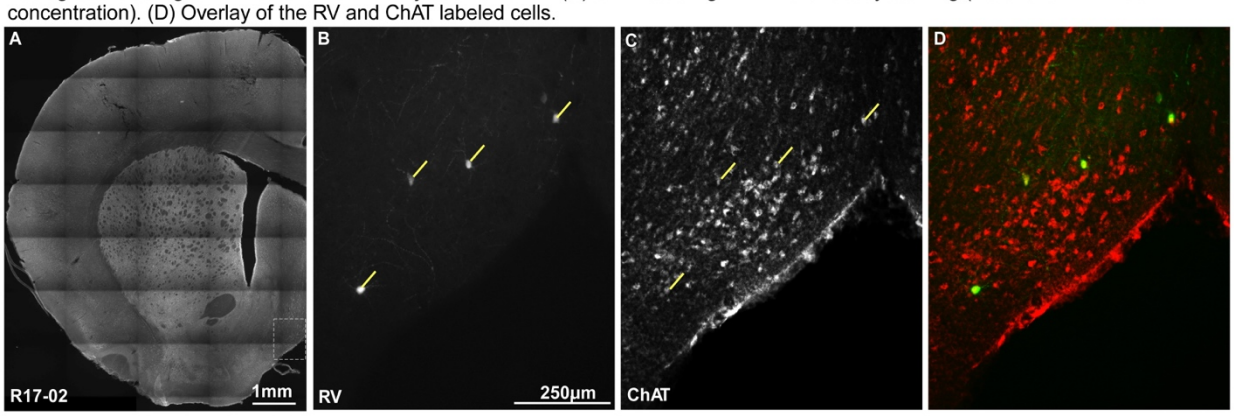

3.2 Results

Immunohistological processing confirmed that the laser fiber did indeed reach the basal forebrain and, specifically, reached cells which were retrogradely labeled from our V1 injection site (Figure 3.2C). Additionally, ChAT antibody stains of basal forebrain neurons co-labeled our retrogradely labeled projection neurons, confirming the cholinergic nature of these cells (Figure 3.3).

3.2a Spike Frequency at Optimal Stimulus Size Decreases with BF Stimulation

31 cells were analyzed for the firing rate at the optimal aperture across 3 different laser conditions and a control condition. All other stimulus parameters, orientation, spatial frequency, etc., remained constant across the four different conditions. There was a significant decrease in firing rate across all 3 laser conditions compared with the control condition (Figure 3.4A, $p<0.002$ at 5mW, $p<0.007$ at 10mW, $p<0.05$ at 15mW). This is consistent with our expectation that increased basal forebrain activity and subsequent increased acetylcholine release causes an increase in inhibitory neuron activity and therefore decrease in firing rate of V1 principle neurons. This expectation is based on our previous finding that basal forebrain inputs to V1 directly target inhibitory neurons, but not excitatory neurons (Lean et al., 2019).

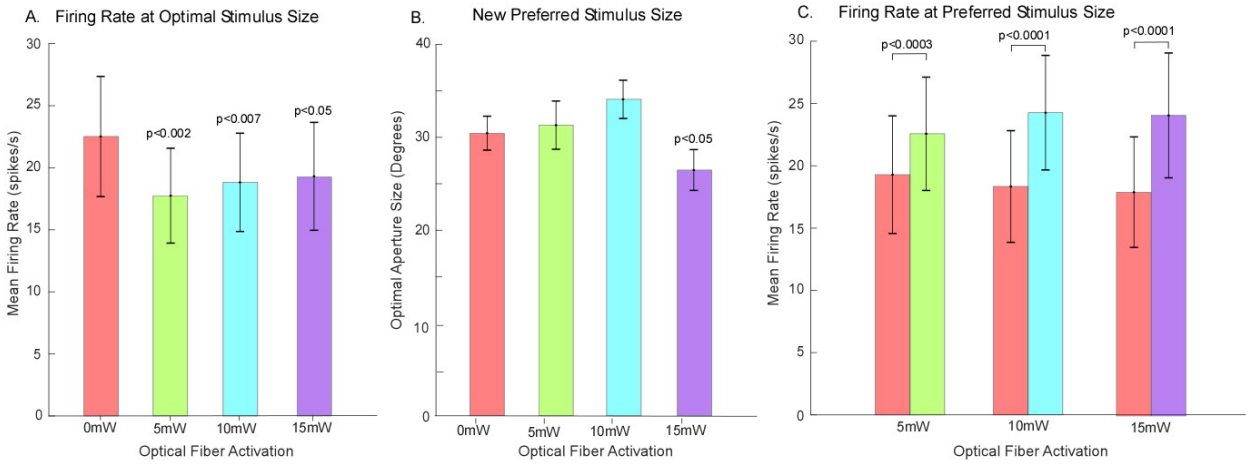

Figure 3.4: (A) Average spike frequency across 31 cells at control and increasing laser conditions at the cell's preferred aperture with no laser. Note that there is a significant different between the firing rate at the control (0mW) condition and all three laser conditions. (B) Change in preferred stimulus size from control condition. Note that the difference between the control and highest laser power (15mW) was significant ($p<0.05$). (C) Firing rate at the control (red bar) and laser conditions at the preferred size for each condition. Note that the firing rate at each stimulus size is lower than the firing rate for the laser condition.

3.2b Change in Optimal Stimulus Size at Highest BF Activation

In addition to a decrease in spike frequency at the cell's preferred stimulus size, there was a noted change in the preferred size with basal forebrain activation (Figure 3.4B). Specifically, there was a significant decrease between the optimal stimulus size at the maximum laser activation used compared with the control condition (15mW; $p<0.05$).

3.2c Laser-Induced Increase in Firing Rate at New Optimal Size

At the new preferred stimulus size for each laser condition, we compared the firing rate with that of the no-laser condition at the same size. Here, we note that the firing rate in the no-laser condition at these sizes is significantly lower than that of the laser condition (Figure 3.4C). Additionally, the difference between the two continues to grow, indicating that the basal forebrain stimulation is causing V1 cell suppression with smaller sizes and enhancing the cell's firing rate at that stimulus.

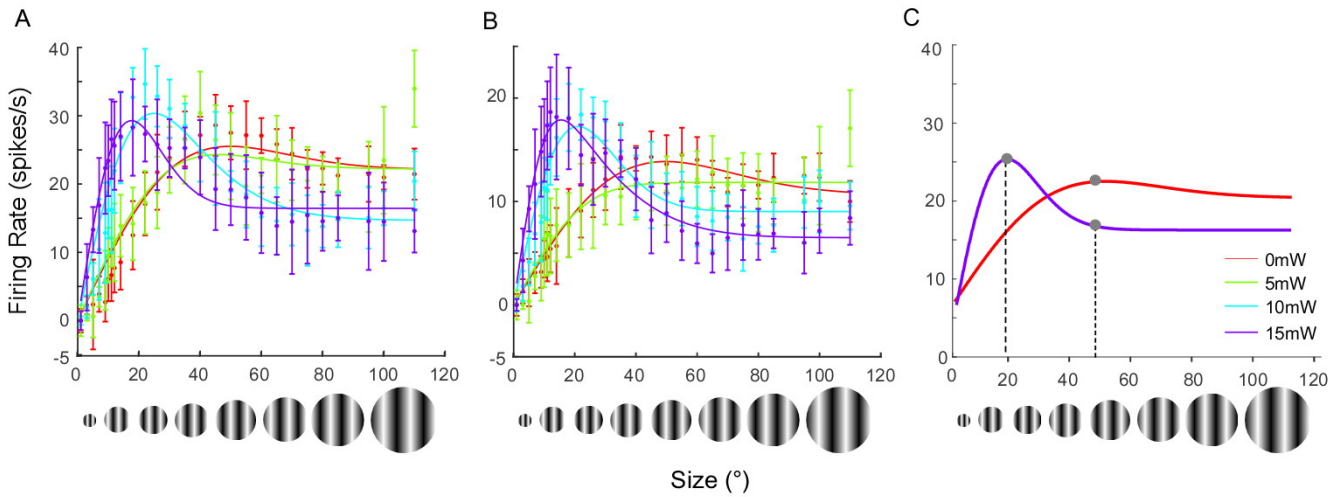

Figure 3.5: (A,B) Example cells of firing rate change at varying stimulus sizes (depicted) with varying laser activation (red=control, green=5mW, blue=10mW, purple=15mW). (C) Analysis of 31 cells led to the conclusion that BF activation causes a decrease in the preferred stimulus size and a suppression of the firing rate at the cell's preferred size with no modulation.

The general trend in firing rate across increasing aperture sizes with 4 different conditions is summarized in figure 3.5. Data from two exemplar cells is shown in figure 3.5A and 3.5B. A summary diagram of the population activity for no laser and maximum laser is shown in figure 3.5C. Given the shift toward a smaller preferred stimulus size and a decrease in the firing rate at the cell's optimal size at control conditions, we can depict the change in firing rate according to the relationship shown.

3.2d Depth Effects on Spike Frequency Differences

Finally, the relationship between cortical depth and stimulus preference was examined in order to further study the previously noted laminar differentiation (Disney et al., 2012; Soma et al., 2013; Rieck & Carey, 1984; Sato et al., 1987b). The firing rates of 31 cells at optimal stimulus orientation across different cortical depths were compared between a zero-laser and a 15mW laser condition. These results revealed a consistent pattern of decreased firing rate across all cortical levels, with a significant decrease in the firing rate at cortical depths ranging from

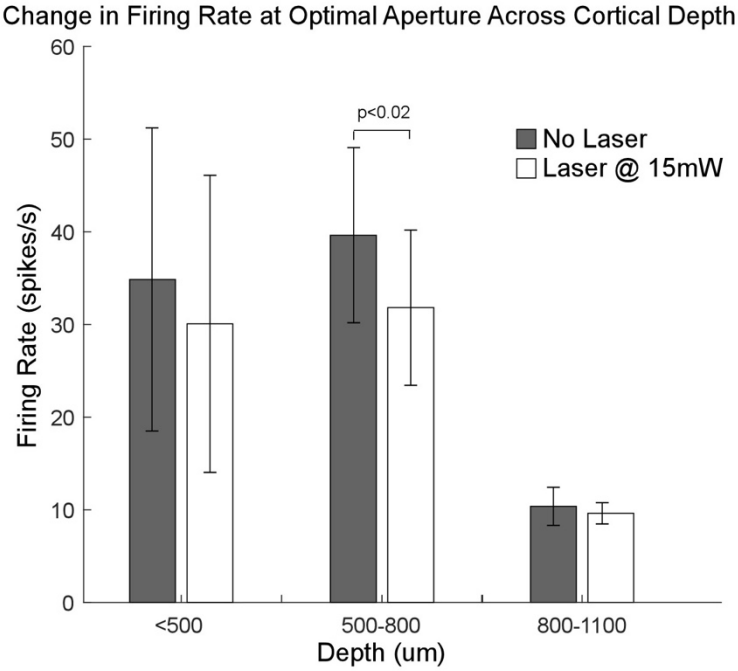

Figure 3.6: Average firing rate change (N=31) between control (0mW) condition and maximum (15mW) laser condition across 3 different cortical depths. Though the firing rate decreased across all cortical depths, the change in firing rate was significantly decreased in the middle layers.

500-800μm (Figure 3.6; $p<0.02$). Although these results are preliminary, they suggest distinct functional roles at different cortical levels.

3.3 Discussion

The results demonstrated above show a modulatory relationship between direct basal forebrain stimulation via optogenetic manipulation and firing rate of V1 cells at specific stimulus sizes. These results are consistent with the proposed understanding of basal forebrain's role in cholinergic modulation of predominantly inhibitory neurons in V1 (Lean et al., 2019; Henderson, 1981; Tigges et al., 1982; Carey & Rieck, 1987; Dreher, Dehay, & Bullier, 1990; Do et al., 2016; Disney et al., 2012). An increase in basal forebrain activation leads to subsequent acetylcholine release in V1; inhibitory neurons with cholinergic receptors are stimulated and this causes a shift in the preferred stimulus size and inhibition at the cell's non-modulated preferred stimulus (Figure 3.5C).

Further evidence for the cholinergic nature of this projection lie in the negative results found across our data set. Upon analysis, no significant change in orientation and direction selectivity was noted to correlate with basal forebrain stimulation. This is consistent with prior results from Sato et al. (1987b), who noted no change to orientation and direction selectivity of cortical cells following depletion of acetylcholine.

Prior studies have focused mainly on the role of acetylcholine release via iontophoresis and examined a change in contrast gain (Soma et al., 2013; Disney et al., 2012) and spatial integration (Roberts et al., 2005). These changes have been noted in studies involving acetylcholine application, as opposed to the direct stimulation of cholinergic release in vivo. It is possible that the effects seen with direct cholinergic application are related to the amount of acetylcholine released, which was not measured in this experimental procedure. It is likely that the pathway activation releases a smaller amount of acetylcholine, and as such the resulting effects are different. This would explain the insignificant changes in contrast gain seen in our experimental protocol.

Additionally, other studies have noted laminar differentiation (Sato et al., 1987b; Soma et al., 2013; Disney et al., 2012; Sato et al., 1987b), but have not shown a clear depth effect with cholinergic modulation or basal forebrain stimulation. Here, we demonstrate that there is a significant change in firing rate with increased basal forebrain stimulation in the middle cortical layers, but likely more data is required to conclude whether such effects are limited to just these cortical layers. The potential for cortical differentiation is critical in determining the role of acetylcholinergic-based modulation for different receptor types; specifically, the effect of activation causing release of acetylcholine to nicotinic receptors in layer 4 (Disney et al., 2006; Disney et al., 2007; Soma et al., 2013; Thiele, 2009).

It is worth noting that we also performed experiments using the inhibitory opsin, archaerhodopsin-3 TP009 (ArchT), to inactivate the basal forebrain projection pathway, as was done by Pinto et al. (2013). However, no notable changes were detected in firing rates in these cases. Unlike Pinto’s protocol, which required behavioral responses to measure the effect of this projection, our protocol was completed while the animal was under light anesthesia and did not require a behavioral component; therefore, the anaesthetized animal was already in a suppressed state of arousal and will have a lower baseline that will not reflect further suppression via optogenetic inactivation.

These results provide direct evidence of modulation via BF connections to V1 and support the proposed understanding of attentional effects in the cortex. Attending to a particular stimulus requires increased sensory representation toward the object of interest and decreased activation to the non-attended stimulus (Deco & Thiele, 2009; Spitzer et al., 1988; Motter, 1993; Treue & Maunsell, 1996; Roelfsema et al., 1998; Roberts et al., 2007; Reynolds et al., 2009). Therefore, the increased activation at a smaller stimulus size and a reduction in firing rate at the larger sizes shown here are a direct result of endogenous cholinergic release in vivo.

CHAPTER 4: SUMMARY AND CONCLUSIONS

The ability to successfully interpret external stimuli depends on the healthy function of the cholinergic system (Newman et al., 2012; Sarter et al., 2005; Hasselmo & Sarter, 2011; Klinkenberg et al., 2011). Most of our knowledge about central cholinergic function in cognition has come from lesion and pharmacological studies (Sato et al, 1987a; Sato et al., 1987b; Everitt and Robbins, 1997; McGaughy et al., 2000; Hasselmo and Sarter, 2011) or external iontophoretic application of acetylcholine (Sato et al., 1987a; Sato et al., 1987b; Roberts et al., 2005; Soma et al., 2013; Disney et al., 2012; Bhattacharyya et al., 2013). With the more recent advent of targeted genetic mutations and cell-type specific tracing techniques, our ability to examine projection patterns in detail has grown significantly (Wickersham et al., 2007; Wickersham et al., 2010; Liu et al., 2013; Liu et al, 2014; Osakada et al., 2011; Kim et al., 2016).

The basal forebrain provides cholinergic inputs to primary visual cortex (V1) that play a key modulatory role on visual cognition (Bear & Singer, 1986; Bhattacharyya et al., 2013; Carey & Rieck, 1987; Chubykin et al., 2013; Everitt & Robbins, 1997; Goard & Dan, 2009; Hasselmo & Sarter, 2011; Henderson, 1981; Herrero et al., 2008; Klinkenberg et al., 2011; Lin et al., 2015; Reynolds & Heeger, 2009; Sarter et al., 2005; Sillito et al., 1983; Soma et al., 2013). While basal forebrain afferents terminate in the infragranualar layers of V1, acetylcholine is delivered to more superficial layers through volume transmission (Descarries et al., 1997; Sarter et al., 2009). Nevertheless, direct synaptic contact in deep layers 5 and 6 may provide a more immediate effect on V1 modulation (Carey & Rieck, 1987; Rieck & Carey, 1984).

Summary of results:

Based on the results presented here, it is clear that the rodent visual cortex is subject to extensive neuromodulation from the basal forebrain. The data presented above supports the conclusion that basal forebrain projection neurons synapse directly onto inhibitory neurons in V1, with no notable input to excitatory cells. Use of an optimized virus increased the amount of retrograde tracing that was visible following similar protocols. It is likely that this increase in tracing is the result of better infection and less toxicity of cortical neurons (Kim et al., 2016).

Following anatomical analysis of the projection type and strength, inhibitory modulation was then shown in vivo using electrophysiological recordings during optogenetic stimulation of basal forebrain neurons. Significant suppression of cell response to preferred stimuli was shown during basal forebrain activation and peak firing rate of V1 neurons was found with smaller stimuli during laser conditions. These results support the anatomical work by indicating a greater effect of basal forebrain neurons on V1 inhibition, rather than excitation.

Limitations:

Though the results here are significant in determining the circuitry underlying the functional role of attentional modulation in V1, there are certain limitations with the methodology. First, it is difficult to confirm the location of the laser during optogenetic stimulation, due to the large area covered by the BF and the lack of cortical landmarks that correspond with BF regions. Though we can confirm proper location via immunohistochemical analysis post mortem, we have limited ability to know with certainty that our laser is successfully reaching pre-synaptically labeled neurons in BF.

Second, there is variability in cortical depth across different animals; that is, each layer of the visual cortex of one animal may be shallower or extend deeper than the standard rat atlas

suggests. Additionally, the electrode may compress the cortex upon initial introduction and then shift further as the tissue settles around the fiber. This makes comparison across layers difficult because the exact layer is not known. Nevertheless, cortical distinction is an important component of this circuit (Disney et al., 2012) and should be the focus of additional studies.

Another limitation that must be noted is the lack of behavioral analysis as part of our attentional modulation paradigm. Behavioral studies with BF activation and acetylcholine application have been shown (Pinto et al., 2013; Roberts et al., 2007; Roelfsema et al., 1998; Motter, 1993; Bear & Singer, 1986; Chubykin et al., 2013) and were not the goal of this study; our goal was primarily to determine the specific circuitry involved in this pathway and the effect this has on V1 neuron parameters. By examining the change in a cell's preferred firing rate to a stimulus presented, we are able to analyze the specific role this pathway has on attentional modulation without a behavioral component.

Implications in Attentional Modulation Processing:

The implications of these results and future related studies are critical to our understanding of attention and its role in modulating neurophysiological processes. Behavioral studies of attention have demonstrated that iontophoretic application of acetylcholine causes overall improved responsiveness to visual inputs (Pinto et al., 2013; Roberts et al., 2007; Bear & Singer, 1986; Chubykin et al., 2013). Here, we demonstrate the ability to study the same process by tapping into the endogenous acetylcholinergic pathways in vivo with direct labeling methods. Specifically, we provide evidence for fine-tuning of firing rate and preferred stimulus size in single V1 neurons, which is an example of cholinergic release via attentional modulation can affect early sensory processing.

These results are consistent with the normalization model of attention (Reynolds & Heeger, 2009). Activation of inhibitory neurons via acetylcholine release causes increased suppression, therefore decreasing the cell's firing rate for the preferred stimulus and shifting the receptive field preference. These results may have possible implications for the development of therapeutic aids of attention-related disorders, as this activation allows for more detailed resolution of the visual stimulus and overall suppression of surrounding context.

References

Ahmed, B., Anderson, J.C., Douglas, R.J., Martin, K.A., & Nelson, J.C. (1994). Polyneuronal innervation of spiny stellate neurons in cat visual cortex. *J Comp Neurol.* 341, 39–49.

Albus, K. (1981). Hypothalamic and basal forebrain afferents to the cat's visual cortex: a study with horseradish peroxidase. *Neuroscience letters 24*(2), 117–21.

Anderson, J.C., Douglas, R.J., Martin, K.A., & Nelson, J.C. (1994). Synaptic output of physiologically identified spiny stellate neurons in cat visual cortex. *J Comp Neurol.* 341, 16–24.

Angelucci, A., Levitt, J.B., Walton, E.J., Hupe, J.M., Bullier, J., & Lund, J.S. (2002). Circuits for local and global signal integration in primary visual cortex. *J Neurosci*. 22:8633--8646.

Attallah, B. V., Bruns, W., Carandini, M., & Scanziani, M. (2012). Parvalbumin-expressing interneurons linearly transform cortical responses to visual stimuli. *Neuron,* 73, 159-170.

Avery, M., Krichmar, J., & Dutt, N. (2012, June 10-15). Spiking neuron model of basal forebrain enhancement of visual attention. Paper presented at the IEEE World Congress on Computational Intelligence, Brisbane, Australia.

Bear, M. F., & Singer, W. (1986). Modulation of visual cortical plasticity by acetylcholine and noradrenaline. *Nature*, 320, 172 ‑ 176.

Bhattacharyya, A., Veit, J., Kretz, R., Bondar, I., & Rainer, G. (2013). Basal forebrain activation controls contrast sensitivity in primary visual cortex. *BMC Neuroscience, 14(1),* 55.

Brainard, D.H. (1997). The Psychophysics Toolbox. *Spat Vis 10:*433-436.

Callaway, E.M. (2005). Structure and function of parallel pathways in the primate early visual system. *The Journal of Physiology*, *566*(1), 13–19.

Callaway, E.M., & Luo, L. (2015). Monosynaptic circuit tracing with glycoprotein-deleted rabies viruses. *J. Neurosci.* 35, 8979-8985.

Carey, R. G., & Rieck, R. W. (1987). Topographic projections to the visual cortex from the basal forebrain in the rat. *Brain Research*, 424, 205–215.

Casagrande, V. A. (1994). A third parallel visual pathway to primate area V1. *Trends in Neurosciences*, 17, 305–310.

Casagrande, V. A., & Harting, J. K. (1975). Transneuronal transport of titrated fucose and proline in the visual pathways of tree shrew Tupaia glis. *Brain Research*, 96, 367–372.

Casagrande, V. A., Sary, G., Royal, D., & Ruiz, O. (2005). On the impact of attention and motor planning on the lateral geniculate nucleus. *Progress in Brain Research,* 149, 11–29.

Casagrande, V. A., Xu, X., & Sary, G. (2002). Static and dynamic views of visual cortical organization. *Progress in Brain Research*, 136, 389–408.

Cavanaugh, J.R., Bair, W., & Movshon, J.A. (2002). Nature and interaction of signals from the receptive field center and surround in macaque V1 neurons. *J Neurophysiol*. 88:2530-2546.

Chen, G., Dan, Y., & Li, C.Y. (2005). Stimulation of non-classical receptive field enhances orientation selectivity in the cat. *J Physiol*. 564:233--243.

Chubykin, A. A., Roach, E. B., Bear, M. F., & Shuler, M. G. H. (2013). A cholinergic mechanism for reward timing within primary visual cortex. *Neuron,* 77, 723–735.

Connolly, J. D., Hashemi-Nezhad, M., & Lyon, D. C. (2012). Parallel feedback pathways in visual cortex of cats revealed through a modified rabies virus. *The Journal of Comparative Neurology,* 520, 988 ‑ 1004.

Das, A., & Gilbert, C. (1999). Topography of contextual modulations mediated by short-range interactions in primary visual cortex. *Nature* 399(6737), 655-661.

Dasari, S., & Gulledge, A.T. (2011). M1 and M4 receptors modulate hippocampal pyramidal neurons. *J. Neurophysiol.* 105, 779-792.

Deco, G, & Thiele, A. (2009). Attention–oscillations and neuropharmacology. *European journal of neuroscience* 30, 347-354.

Descarries, L., Gisiger, V., & Steriade, M. (1997). Diffuse transmission by acetylcholine in the CNS. *Prog. Neurobiol.* 53, 603-625.

Disney, A. A., & Aoki, C. (2008). Muscarinic acetylcholine receptors in macaque V1 are most frequently expressed by parvalbumin-immunoreactive neurons. *The Journal of comparative neurology*, *507*(5), 1748–1762.

Disney, A.A., Aoki, C., & Hawken, M.J. (2012). Cholinergic suppression of visual responses in primate V1 is mediated by GABAergic inhibition. *Journal of neurophysiology* 108, 1907-1923.

Disney, A.A., Aoki, C., & Hawken, M.J. (2007). Gain modulation by nicotine in macaque v1. *Neuron* 56, 701-713.

Disney, A.A., Domakonda, K.V., & Aoki, C. (2006). Differential expression of muscarinic acetylcholine receptors across excitatory and inhibitory cells in visual cortical areas V1 and V2 of the macaque monkey. *The Journal of comparative neurology 499*(1), 49 ‐ 63.

Disney, A.A., & Reynolds, J.H. (2014). Expression of m1-type muscarinic acetylcholine receptors by parvalbumin-immunoreactive neurons in the primary visual cortex: a comparative study of rat, guinea pig, ferret, macaque, and human. *The Journal of comparative neurology, 522*(5), 986–1003.

Do, J., Xu, M., Lee, S.-H., Chang, W.-C., Zhang, S., Chung, S., Yung, T., et al. (2016). Cell type-specific long-range connections of basal forebrain circuit. *eLife*, *5*, e13214. elife.

Dreher, B., Dehay, C., & Bullier, J. (1990). Bihemispheric collateralization of the cortical and subcortical afferents to the rat's visual cortex. *The European Journal of Neuroscience*, 2, 317–331.

Everitt, B.J., & Robbins, T.W. (1997). Central cholinergic systems and cognition. *Annual review of psychology 48*, 649–84.

Felleman, D. J., & Van Essen, D. C. (1991). Distributed hierarchical processing in the primate cerebral cortex. *Cereb Cortex,* 1, 1–47.

Fitzpatrick, D., Carey, R.G., & Diamond, I.T. (1980). The projection of the superior colliculus upon the lateral geniculate body in *Tupaia glis* and Galago senegalensis. *Brain Research, 194,* 494-499.

Foik, A. T., Lean, G. A., Scholl, L. R., & Lyon, D.C. (2016, November). *Receptive field properties of single neurons in the lateral posterior nucleus of the rat.* Poster presented at the Society for Neuroscience Conference, San Diego, CA.

Goard, M., & Dan, Y. (2009). Basal forebrain activation enhances cortical coding of natural scenes. *Nature Neuroscience*, 12, 1444–1449.

Guillery, R. W., & Sherman, S. M. (2002). Thalamic relay functions and their role in corticocortical communication: generalizations from the visual system. *Neuron*, 33, 163–175.

Han X., & Boyden E.S. (2007). Multiple-color optical activation, silencing, and desynchronization of neural activity, with single-spike temporal resolution.ES.*PLoS One.* 2(3), e299.

Hashemi-Nezhad, M., & Lyon, D. C. (2012). Orientation tuning of the suppressive extraclassical surround depends on intrinsic organization of V1. *Cerebral Cortex*, 22, 308–326.
Hasselmo, M.E., & Sarter, M. (2011). Modes and models of forebrain cholinergic neuromodulation of cognition. *Neuropsychopharmacology Reviews* 36, 52-73.
Henderson, Z. (1981). A projection from acetylcholinesterase-containing neurones in the diagonal band to the occipital cortex of the rat. *Neuroscience,* 6, 1081–1088.
Hendry, S.H., Schwark, H.D., Jones, E.G., & Yan, J. (1987). Numbers and proportions of GABA-immunoreactive neurons in different areas of monkey cerebral cortex. *J Neurosci.* 7, 1503-1519.
Herrero, J.L., Roberts, M.J., Delicato, L.S., Gieselmann, M.A., Dayan, P., & Thiele, A. (2008). Acetylcholine contributes through muscarinic receptors to attentional modulation in V1. *Nature 454(*7208), 1110-1114.
Hirsch, J.A., Gilbert, C.D. (1991) Synaptic physiology of horizontal connections in the cat's visual cortex. *J. Neurosci.* 11, 1800–1809.
Imua, K., & Rockland, K.S. (2006). Long-range interneurons within the medial pulvinar nucleus of macaque monkeys. *The Journal of Comparative Neurology, 498,* 649-666.
Jones, B.E. (2004). Activity, modulation and role of basal forebrain cholinergic neurons innervating the cerebral cortex. *Progress in brain research 145*, 157–169.
Jones, H.E., Grieve, K.L., Wang, W., & Sillito, A.M. (2001). Surround suppression in primate V1. *J Neurophysiol.* 86, 2011-2028.
Kaas, J. H. (2012). Evolution of columns, modules, and domains in the neocortex of primates. *Proceedings of the National Academy of Sciences of the United States of America*, 109, 10655–10660.
Kaas, J.H., & Lyon, D.C. (2007). Pulvinar contributions to the dorsal and ventral streams of visual processing in primates. *Brain Research Reviews, 55,* 285-296.
Kim, E. J., Jacobs, M. W., Ito-Cole, T., & Callaway, E.M. (2016). Improved monosynaptic neural circuit tracing using engineered rabies virus glycoproteins. *Cell Reports,* 15, 692-699.
Kleiner, M., Brainard, D., Pelli, D., Ingling, A., Murray, R., & Broussard, C. (2007). What's new in psychtoolbox-3. *Perception* 36:1-16.
Klinkenberg, I., Sambeth, A., & Blokland, A. (2011). Acetylcholine and attention. *Behavioral Brain Research, 221(2),* 430-442.
Krubitzer, L., Campi, K. L., & Cooke, D. F. (2011). All rodents are not the same: A modern synthesis of cortical organization. *Brain, Behavior and Evolution*, 78, 51–93.
Lachica, E.A., & Casagrande, V.A. (1992). Direct W-like geniculate projections to the cytochrome oxidase (CO) blobs in primate visual córtex: Axon morphology. *The Journal of Comparative Neurology, 319,* 141-158.
Lean, G.A., Liu, Y.J., & Lyon, D.C. (2015, November). *Cell-type specific tracing of the subcortical input to primary visual cortex from the hypothalamus.* Poster presented at the Society for Neuroscience Conference, Chicago, IL.
Lean, G. A., Liu, Y.-J., & Lyon, D. C. (2019). Cell type specific tracing of the subcortical input to primary visual cortex from the basal forebrain. *The Journal of Comparative Neurology*, 527(3). https://doi.org/10.1002/cne.24412
Letzkus, J.J., Wolff, S.B., Meyer, E.M., Tovote, P., Courtin, J., Herry, C., Lüthi, A. (2011). A disinhibitory microcircuit for associative fear learning in the auditory cortex. *Nature* 480, 331-335.

Lin, S.C., Brown, R.E., Shuler, M.G.H., Petersen, C.C.H., Kepecs, A. (2015). Optogenetic dissection of the basal forebrain neuromodulatory control of cortical activation, plasticity, and cognition. *The Journal of Neuroscience 35*(41), 13896-13903.

Liu, Y.J., Arreola, M., Coleman, C., & Lyon, D. (2014). Very-long-range disynaptic V1 connections through layer 6 pyramidal neurons revealed by transneuronal tracing with rabies virus. *Eye and Brain, 6,* 45-56.

Liu, Y.-J., Ehrengruber, M. U., Negwer, M., Shao, H.-J., Cetin, A. H., & Lyon, D. C. (2013). Tracing inputs to inhibitory or excitatory neurons of mouse and cat visual cortex with a targeted rabies virus. *Current Biology*, 23, 1746–1755.

Liu, Y.-J., Hashemi-Nezhad, M., & Lyon, D. C. (2011). Dynamics of extraclassical surround modulation in three types of V1 neurons. *Journal of Neurophysiology*, 105, 1306–1317.

Lucas-Meunier, E., Monier, C., Amar, M., Baux, G., Frégnac, Y., & Fossier, P. (2009). Involvement of nicotinic and muscarinic receptors in the endogenous cholinergic modulation of the balance between excitation and inhibition in the young rat visual cortex. *Cerebral Cortex 19*(10), 2411–27.

Lyon, D. C., Jain, N., & Kaas, J. H. (1998). Cortical connections of striate and extrastriate visual areas in tree shrews. *The Journal of Comparative Neurology*, 401, 109–128.

Lyon, D. C., Jain, N., & Kaas, J. H. (2003a). The visual pulvinar in tree shrews II. Projections of four nuclei to areas of visual cortex. *The Journal of Comparative Neurology, 467,* 607-627.

Lyon, D. C., Jain, N., & Kaas, J. H. (2003b). The visual pulvinar in tree shrews I. Multiple subdivisions revealed through acetylcholinesterase and Cat-301 chemoarchitecture. *The Journal of Comparative Neurology, 467,* 593-606.

Lyon, D.C., Nassi, J.J., & Callaway, E.M. (2010). A disynaptic relay from superior colliculus to dorsal stream visual cortex in macaque monkey. *Neuron, 65,* 270-279.

Lyon, D.C., & Rabideau, C. (2012). Lack of robust LGN label following transneuronal rabies virus injections into macaque area V4. *The Journal of Comparative Neurology, 520,* 2500-2511.

Lyon, D. C., Xu, X., Casagrande, V. A., Stefansic, J. D., Shima, D., & Kaas, J. H. (2002). Optical imaging reveals retinotopic organization of dorsal V3 in New World owl monkeys. *Proceedings of the National Academy of Sciences of the United States of America*, 99, 15735–15742.

Lysakowski, A., Wainer, B. H., Bruce, G., & Hersh, L. B. (1989). An atlas of the regional and laminar distribution of choline acetyltransferase immunoreactivity in rat cerebral cortex. *Neuroscience,* 28, 291–336.

Marshel, J. H., Garrett, M. E., Nauhaus, I., & Callaway, E. M. (2011). Functional specialization of seven mouse visual cortical areas. *Neuron*,72, 1040–1054.

Marshel, J.H., Kaye, A.P., Nauhaus, I., & Callaway, E.M. (2012). Anterior-posterior direction opponency in the superficial mouse lateral geniculate nucleus. *Neuron, 76,* 713-720.

Martinez-Trujillo, J., & Treue, S. (2002). Attentional modulation strength in cortical area MT depends on stimulus contrast. *Neuron, 35,* 365-370.

McAdams, C.J., & Maunsell, J.H.R. (1999). Effects of attention on orientation-tuning functions of single neurons in macaque cortical area V4. *The Journal of Neuroscience, 19*(1), 431-441.

McGaughy, J., Everitt, B.J., Robbins, T.W., & Sarter, M. (2000). The role of cortical cholinergic

afferent projections in cognition: impact of new selective immunotoxins. *Behavioral Brain Research, 115(*2), 251-263.

Mechawar, N., Cozzari, C., & Descarries, L. (2000). Cholinergic innervation in adult rat cerebral cortex: A quantitative immunocytochemical description. *The Journal of Comparative Neurology*, 428, 305 ‑ 318.

Mesulam, M.M., Mufson, E.J., Wainer, B.H., & Levey, A.I. (1983a). Central cholinergic pathways in the rat: an overview based on an alternative nomenclature (Ch1–Ch6). *Neuroscience, 10*(4), 1185-1201.

Mesulam, M.M., Mufson, E.J., Levey, A.I., & Wainer, B.H. (1983b). Cholinergic innervation of cortex by the basal forebrain: cytochemistry and cortical connections of the septal area, diagonal band nuclei, nucleus basalis (substantia innominata), and hypothalamus in the rhesus monkey. *The Journal of comparative neurology*, *214*(2), 170–197.

Meynert, T.H. (1872). The brain of mammals. In: A manual of histology (Stricker S, ed), pp 650-766. New York: Wood.

Miyamichi, K., Shlomai-Fucks, Y., Shu, M., Weissbourd, B.C., Luo, L., & Mizrahi, A. (2013). Dissecting local circuits: parvalbumin interneurons underlie broad feedback control of olfactory bulb output. *Neurons* 80, 1232-1245.

Motter, B.C. (1993). Focal attention produces spatially selective processing in visual cortical areas V1, V2, and V4 in the presence of competing stimuli. *J. Neurophysiol., 70,* 909-919.

Mrzljak, L., Levey, A.I., & Goldman-Rakic, P.S. (1993). Association of m1 and m2 muscarinic receptor proteins with asymmetric synapses in the primate cerebral cortex: morphological evidence for cholinergic modulation of excitatory neurotransmission. Proc Natl Acad Sci USA 93, 7337-7340.

Muir, J.L., Everitt, B.J., & Robbins, T.W. (1994). AMPA-induced excitotoxic lesions of the basal forebrain: a significant role for the cortical cholinergic system in attentional function. *The Journal of Neuroscience: the official Journal of the Society for Neuroscience*, *14*(4), 2313–2326.

Nassi, J.J., Lyon, D.C., & Callaway, E.M. (2006). The parvocellular LGN provides a robust disynaptic input to the visual motion area MT. *Neuron, 50,* 319-327.

Nathanson, J.L., Yanagawa, Y., Obata, K., & Callaway, E.M. (2009). Preferential labeling of inhibitory and excitatory cortical neurons by endogenous tropism of adeno-associated virus and lentivirus vectors. *Neuroscience, 161,* 441-450.

Negwer, M., Liu, Y. J., Schubert, D., & Lyon, D. C. (2017). V1 connections reveal a series of elongated higher visual areas in the California ground squirrel, Otospermophilus beecheyi. *The Journal of Comparative Neurology*, 525, 1909–1921.

Newman, E. L., Gupta, K., Climer, J. R., Monaghan, C. K., & Hasselmo, M. E. (2012). Cholinergic modulation of cognitive processing: Insights drawn from computational models. *Frontiers in Behavioral Neuroscience*, 6, 1–19.

Niell, C. M. (2015). Cell types, circuits, and receptive fields in the mouse visual cortex. *Annual Review of Neuroscience*, 38, 413–431.

Osakada, F., Mori, T., Cetin, A., Marshel, J., Virgen, B., & Callaway, E. (2011). New rabies virus variants for monitoring and manipulating activity and gene expression in defined neural circuits. *Neuron*, *71*(4), 617–631.

Paxinos, G., & Franklin, K.B.J. (2001). *The mouse brain in stereotaxic coordinates (*2nd ed). San Diego, CA: Academic Press.

Pelli, D.G. (1997). The Video Toolbox software for visual psychophysics: transforming numbers into movies. *Spat Vis* 10:437-442.

Pinto, L., Goard, M., Estandian, D., Xu, M., Kwan, A., Lee, S.-H., Harrison, T., Feng, G. & Dan, Y. (2013). Fast modulation of visual perception by basal forebrain cholinergic neurons. *Nature Neuroscience*, *16*(12), 1857–63.

Purushothaman, G., Marion, R., Li, K., & Casagrande, V.A. (2012). Gating and control of primary visual cortex by pulvinar. *Nature Neuroscience, 15,* 905-912.

Reid, R.C., & Alonso, J.-M. (1995). Specificity of monosynaptic connections from thalamus to visual cortex. *Nature,* 378, 281–284.

Reynolds, J.H., & Heeger, D.J. (2009). The normalization model of attention. *Neuron, 61,* 168-185.

Reynolds, J.H., Chelazzi, L., & Desimone, R. (1999) Competitive mechanisms subserve attention in macaque areas V2 and V4. *J. Neurosci., 19,* 1736-1753.

Reynolds, J.H., Pasternak, T., & Desimone, R. (2000). Attention increases sensitivity of V4 neurons. *Neuron*, 26, 703-714.

Rieck, R., & Carey, R.G. (1984). Evidence for a laminar organization of basal forebrain afferents to the visual cortex. *Brain Research*, 297, 374-380.

Roberts, M.J., Delicato, L.S., Herrero, J., Gieselmann, M.A., & Thiele, A. (2007) Attention alters spatial integration in macaque V1 in an eccentricity-dependent manner. *Nature Neuroscience, 10,* 1483-1491.

Roberts, M. J., Zinke, W., Guo, K., Robertson, R., McDonald, J. S., & Thiele, A. (2005). Acetylcholine dynamically controls spatial integration in marmoset primary visual cortex. *Journal of neurophysiology*, *93*(4), 2062–2072.

Roelfsema, P.R., Lamme, V.A., & Spekreijse, H. (1998). Object-based attention in the primary visual cortex of the macaque monkey. *Nature, 395,* 376-381.

Sanderson, K.J., Dreher, B., & Gayer, N. (1991). Prosencephalic connections of striate and extrastriate areas of rat visual cortex. *Experimental Brain Research,* 85, 324-334.

Sarter, M., Hasselmo, M. E., Bruno, J. P., & Givens, B. (2005). Unraveling the attentional functions of cortical cholinergic inputs: interactions between signal-driven and cognitive modulation of signal detection. *Brain research reviews*, *48*(1), 98–111.

Sarter, M., Parikh, V. & Howe, W.M. (2009). Phasic acetylcholine release and the volume transmission hypothesis: time to move on. *Nat. Rev. Neurosci.* 10, 383-390.

Sato, H., Hata, Y., Hagihara, K., & Tsumoto, T. (1987a). Effects of cholinergic depletion on neuron activities in the cat visual cortex. *Journal of Neurophysiology, 58,* 781-794.

Sato, H., Hata, Y., Hagihara, K., & Tsumoto, T. (1987b). A functional role of cholinergic innervation to neurons in the cat visual cortex. *Journal of Neurophysiology*, *58*(4), 765–80.

Sceniak, M.P., Ringach, D.L., Hawken, M.J., & Shapley, R. (1999). Contrast's effect on spatial summation by macaque V1 neurons. *Nat Neurosci*. 2,733-739.

Seabrook, T. A., Burbridge, T. J., Crair, M. C., & Huberman, A. D. (2017). Architecture, function, and assembly of the mouse visual system. *Annual Review of Neuroscience,* 40, 499–538.

Sengpiel, F., Sen, A., & Blakemore, C. (1997). Characteristics of surround inhibition in cat area 17. *Exp Brain Res.* 116, 216-228.

Series, P., Lorenceau, J., Fregnac, Y. (2003). The ''silent'' surround of V1 receptive fields: theory and experiments. *J Physiol*, 97, 453–474.

Shuler, M.G., & Bear, M.F. (2006). Reward timing in the primary visual cortex. *Science* 311, 1606-1609.
Shute, C.C.D., & Lewis, P.R. (1967). The ascending cholinergic reticular system: neocortical, olfactory, and subcortical projections. *Journal of Neurology, 90*(3), 497-520.
Sillito, A.M., & Kemp, J.A. (1983). Cholinergic modulation of the functional organization of the cat visual cortex. *Brain Research, 289*(1-2), 143-155.
Silver, M.A., Shenhav, A., & D'Esposito, M. (2008). Cholinergic enhancement reduces spatial spread of visual responses in human early visual cortex. *Neuron*, *60*(5), 904–914.
Soma, S., Shimegi, S., Suematsu, N., & Sato, H. (2013). Cholinergic modulation of response gain in the rat primary visual cortex. *Scientific Reports*, *3*(1), 1138.
Spitzer, H., Desimone, R., & Moran, J. (1988). Increased attention enhances both behavioral and neuronal performance. *Science, 240,* 338-340.
Stepniewska, I., & Kaas, J.H. (1997). Architectonic subdivisions of the inferior pulvinar in New World and Old World monkeys. *Visual Neuroscience, 14,* 1043-1060.
Thomson, A. (2010). Neocortical layer 6, a review. *Frontiers in Neuroanatomy*, *4*, 13.
Tigges, J., Tigges, M., Cross, N. A., McBride, R. L., Letbetter, W. D., & Anschel, S. (1982). Subcortical structures projecting to visual cortical areas in squirrel monkey. *The Journal of Comparative Neurology*, 209, 29 – 40.
Tigges, M., Tigges, J., Rees, H., Rye, D., & Levey, A.I. (1997). Distribution of muscarinic cholinergic receptor proteins m1 to m4 in area 17 of normal and monocularly deprived rhesus monkeys. *J Comp Neurol.* 388, 130-145.
Tohmi, M., Meguro, R., Tsukano, H., Hishida, R., & Shibuki, K. (2014). The extrageniculate visual pathway generates distinct response properties in the higher visual areas of mice. *Current Biology, 24,* 587-597.
Treue, S., & Maunsell, J.H.R. (1996). Attentional modulation of visual motion processing in cortical areas MT and MST. *Nature, 382,* 539-541.
Umbriaco, D., Watkins, K. C., Descarries, L., Cozzari, C., & Hartman, B.K. (1994). Ultrastructural and morphometric features of the acetylcholine innervation in adult rat parietal cortex: an electron microscopic study in serial sections. *J. Comp. Neurol.* 348, 351-373.
Van Brederode, J.F., Mulligan, K.A., & Hendrickson, A.E. (1990). Calcium-binding proteins as markers for subpopulations of GABAergic neurons in monkey striate cortex. *J. Comp. Neurol.* 298, 1-22.
Van Hooser, S.D., & Nelson, S.B. (2006). The squirrel as a rodent model of the human visual system. *Visual Neuroscience, 23,* 765-778.
Vanni, M.P., Thomas, S., Petry, H.M., Bickford, M.E., & Casanova, C. (2015). Spatiotemporal profile of voltage-sensitive dye responses in the visual cortex of tree shrews evoked by electric microstimulation of the dorsolateral geniculate and pulvinar nuclei. *The Journal of Neuroscience, 35,* 11891-11896.
Walker, G.A., Ohzawa, I., & Freeman, R.D. (2000). Suppression outside the classical cortical receptive field. *Vis Neurosci.* 17, 369-379.
Watabe-Uchida, M., Zhu, L., Ogawa, S.K., Vamanrao, A., & Uchida, N. (2012). Whole-brain mapping of direct inputs to midbrain dopamine neurons. *Neurons 74,* 858-873.
Weliky, M., Kandler, K., Fitzpatrick, D., & Katz, L.C. (1995) Patterns of excitation and inhibition evoked by horizontal connections in visual cortex share a common relationship to orientation columns. *Neuron,* 15, 541–552.

Wickersham, I.R., Lyon, D.C., Barnard, R.J., Mori, T., Finke, S., Conzelmann, K.K., Young, J.A., Callaway, E.M. (2007). Monosynaptic restriction of transsynaptic tracing from single, genetically targeted neurons. *Neuron*, 53(5):639-647.

Wickersham, I.R., Sullivan, H.A., & Seung, H.S. (2010). Production of glycoprotein-deleted rabies viruses for monosynaptic tracing and high-level gene expression in neurons. *Nature Protocols, 5,* 595-606.

Wiesel, T.N., & Hubel, D.H. (1966). Spatial and chromatic interactions in the lateral geniculate body of the rhesus monkey. *J Neurophysiol., 29(6),* 1115-1156.

Williford, T. & Maunsell, J.H.R. (2006). Effects of spatial attention on contrast response functions in macaque area V4. *J. Neurophysiol.* 96, 40-54.

Wong, P., & Kaas, J.H. (2008). Architectonic subdivisions of neocortex in the gray squirrel *(Sciurus carolinensis). The Anatomical Record: Advances in Integrative Anatomy and Evolutionary Biology, 291,* 1301-1333.

Wong, P., & Kaas, J.H. (2010). Architectonic subdivisions of neocortex in the galago *(Otolemur garnetti*). *Anatomical Record (Hoboken, N.J.: 2007), 293,* 1033-1069.

Xu, X., Ichida, J.M., Allison, J.D., Boyd, D., Bonds, A.B., & Casagrande, V.A. (2001). A comparison of koniocellular, magnocellular and parvocellular receptive field properties in the lateral geniculate nucleus of the owl monkey *(Aotus trivirgatus). The Journal of Physiology, 531,* 203-218.

Zhang F, Wang LP, Brauner M, Liewald JF, Kay K, Watzke N, Wood PG, Bamberg E, Nagel G, Gottschalk A, Deisseroth K. (2007) Multimodal fast optical interrogation of neural circuitry. *Nature*. 446(7136):633-639.

Zhou, N.A., Maire, P.S., Masterson, S.P., & Bickford, M.E. (2017). The mouse pulvinar nucleus: Organization of the tectorecipient zones. *Visual Neuroscience, 34,* E011.

Zhou, N., Masterson, S., Damron, J., Guido, W., & Bickford, M. (2018). The mouse pulvinar nucleus links the lateral extrastriate cortex, striatum, and amygdala. *The Journal of Neuroscience, 38,* 347-362.